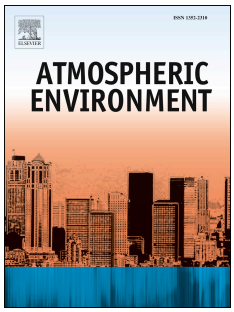

Atmospheric formaldehyde at El Teide and Pic du Midi remote high-altitude sites

Cristina Prados-Roman, Miguel Fernández, Laura Gómez-Martín, Emilio Cuevas, Manuel Gil-Ojeda, Nicolas Marusczak, Olga Puentedura, Jeroen E. Sonke, Alfonso Saiz-Lopez

PII: S1352-2310(20)30352-6

DOI: https://doi.org/10.1016/j.atmosenv.2020.117618

Reference: AEA 117618

To appear in: *Atmospheric Environment*

Received Date: 20 December 2019

Revised Date: 13 May 2020

Accepted Date: 15 May 2020

Please cite this article as: Prados-Roman, C., Fernández, M., Gómez-Martín, L., Cuevas, E., Gil-Ojeda, M., Marusczak, N., Puentedura, O., Sonke, J.E., Saiz-Lopez, A., Atmospheric formaldehyde at El Teide and Pic du Midi remote high-altitude sites, *Atmospheric Environment* (2020), doi: https://doi.org/10.1016/j.atmosenv.2020.117618.

Credit author statement

Cristina Prados-Roman: conceptualization, methodology, formal analysis, investigation, writing – original draft– and visualization. **Miguel Fernández:** investigation and writing – review & editing. **Laura Gómez-Martín:** formal analysis and writing – original draft. **Emilio Cuevas:** formal analysis, writing – review & editing– and visualization. **Manuel Gil-Ojeda:** conceptualization, investigation, writing –review & editing– and funding acquisition. **Nicolas Marusczak:** investigation. **Olga Puentedura:** investigation and writing –review & editing. **Jeroen E. Sonke:** conceptualization, investigation, writing –review & editing– and funding acquisition. **Alfonso Saiz-Lopez:** conceptualization, investigation, writing –review & editing, supervision and funding acquisition.

Atmospheric formaldehyde at El Teide and Pic du Midi remote high-altitude sites

Cristina Prados-Roman [a,1,*], Miguel Fernández [a,2], Laura Gómez-Martín [b], Emilio Cuevas [d], Manuel Gil-Ojeda [b], Nicolas Marusczak [e], Olga Puentedura[b], Jeroen E. Sonke [e], and Alfonso Saiz-Lopez [a, *]

[a] Department of Atmospheric Chemistry and Climate, Institute of Physical Chemistry Rocasolano (CSIC), Madrid, 28006, Spain.
[b] Atmospheric Research and Instrumentation Branch, National Institute for Aerospace Technology (INTA), Madrid, 28850, Spain.
[d] Izaña Atmospheric Research Center (AEMET), Santa Cruz de Tenerife, 38001, Spain.
[e] Observatoire Midi-Pyrénées, Laboratoire Géosciences Environnement Toulouse, CNRS/IRD/Université de Toulouse, Toulouse, 31400, France.
[1] Currently at: Atmospheric Research and Instrumentation Branch, Spanish National Institute for Aerospace Technology (INTA), Madrid, 28850, Spain.
[2] Currently at: Department of Space Sciences and Payloads, Spanish National Institute for Aerospace Technology (INTA), Madrid, 28850, Spain.

Corresponding author: Cristina Prados-Roman (pradosrc@inta.es) and Alfonso Saiz-Lopez (a.saiz@csic.es)

ABSTRACT

Formaldehyde (CH_2O) is a tracer of the photochemical activity of the atmosphere. Linked to air quality, CH_2O is an ozone (O_3) precursor and serves as a proxy for natural and anthropogenic reactive organic emissions. As a product of the photooxidation of methane (CH_4) and other hydrocarbons (e.g., isoprene), CH_2O represents an important source of radicals in the remote free troposphere. This work aims at improving the characterization of this part of the troposphere where data are scarce. In particular, this study assesses the presence of CH_2O at two high-altitude remote sites: El Teide (TEI, 3570 m a.s.l., Tenerife, Canary Islands, Spain) and Pic du Midi (PDM, 2877 m a.s.l., French Pyrenees). Through ground-based remote sensing measurements performed during two field campaigns in July (TEI) and September (PDM) 2013, this study presents the vertical distribution of CH_2O at both locations. Results at PDM show that CH_2O mixing ratios follow a decreasing vertical profile with a mean maximum of 0.5 ± 0.2 nmol mol^{-1} (i.e., ppbv) at the instruments' altitude. At TEI, observations indicate an uplifted layer of CH_2O with a mean maximum of 1.3 ± 0.3 nmol mol^{-1} at 3.8 km a.s.l. (i.e., 300 m above the instrument's altitude). At both remote sites, the observed CH_2O levels are higher than expected for background methane oxidation (a threefold increase in the case of TEI). Air mass back trajectory analysis links CH_2O

observations with abundant natural (e.g. forests) and/or anthropogenic isoprene emissions from the region nearby PDM, while the high CH_2O levels detected at TEI indicate in-plume formation of CH_2O resulting from its precursors emitted from west-African and Canadian fires. Finally, as a key trace gas for O_3 and HO_x chemistries, we estimate the upper limit of bromine monoxide (BrO) in the free troposphere at TEI and PDM to be 0.8 and 1.5 pmol mol^{-1} (i.e., pptv) respectively.

1. Introduction

Formaldehyde (CH_2O) is a volatile organic compound (VOC) that plays an important role in the tropospheric chemistry and budget of O_3, HO_x (OH + HO_2) and NO_x (NO + NO_2). Ubiquitously present in the Earth's atmosphere, formaldehyde's vertical and geographical distribution is not homogenous and has been the subject of investigations for decades. Kitchens et al. (1976) presented a review of CH_2O in polluted environments and its related health risks, while Lowe and Schmidt (1983) addressed the relevance and challenges of measuring CH_2O in the non-urban atmosphere. Currently, CH_2O is considered one of the *Essential Climate Variables* by the WMO (GCOS, 2016) and measurements of its atmospheric abundance are a key for a better understanding of the oxidizing mechanisms in the troposphere, for tracking CH_2O emissions and their embedded hydrocarbon reactions as well as for parametrizing atmospheric chemical and transport models.

Although a small fraction of CH_2O (< 2%) enters the troposphere directly from biomass burning or from anthropogenic or vegetation emissions (Andreae and Merlet, 2001; Olivier et al., 2003; Lathière et al., 2006), most of the CH_2O in the atmosphere is a secondary product of the oxidation of methane (60 %, with a production rate of 1600 Tg/yr) and non-methane hydrocarbons (NMHC), mainly isoprene (~20 %, Stavrakou et al., 2009a; Bates and Jacob, 2019). As for the CH_4 oxidation channel, one of its intermediate products is methyl peroxy radical (CH_3O_2), which proceeds reacting primarily with NO_x (NO + NO_2) in the semi- and polluted atmosphere, yielding methoxy radical (CH_3O) and then CH_2O (Lowe and Schmidt 1983; Wolfe et al., 2016). In unpolluted environments (NO < 20 pmol mol^{-1}), CH_3O_2 reacts with HO_2 forming methyl hydroperoxide (CH_3OOH), eventually yielding CH_2O. In addition to reactions with OH and photolysis (e.g., von Kuhlmann et al., 2003), CH_3OOH can be lost through heterogenous reactions, thus aerosols may indirectly regulate the presence of CH_2O.

Regarding CH_2O loss processes, its main sink is photolysis at $\lambda \leq 350$ nm (Crutzen 1988), resulting in an increase of atmospheric carbon monoxide (CO) which is an ozone precursor. Also, reaction with the hydroxyl radical (OH) and washout and dry deposition can contribute to CH_2O losses (Solberg et al., 2001). As for the CH_2O lifetime, although it can span up to 2 days, in the sunlit atmosphere it is only a few hours (Lowe and Schmidt, 1983; Sander et al., 2006). Due to this short lifetime, CH_2O is often used as a constraint for determining direct emissions of non-methane VOC.

During the last two decades, global tropospheric columns of CH_2O have been intensively monitored by different satellites (GOME/ERS2, SCIAMACHY/Envisat, GOME2/MetOp, OMI/Aura, TROPOMI/S5P; e.g., Chance et al., 2000; De Smedt et al., 2018) aiming at characterizing the tropospheric chemical processes, mainly those linked to air quality or climate change (Schroeder et

al., 2016). In fact, CH_2O is one of the very few VOC that can be detected by satellite and several studies have aimed at determining VOC emissions at a global scale using CH_2O satellite observations (Palmer et al., 2003; Stavrakou et al., 2009a, b; Bauwens et al., 2016) often assisted by numerical models. Also, by means of satellite observations of CH_2O along with chemical models, the distribution of OH in the remote troposphere can be inferred (Wolfe et al., 2019). The down-scaling effort of the satellite and model community to understand CH_2O and the oxidizing mechanisms within emission plumes makes essential the characterization of pristine areas since in those regions the low signal-to-noise ratio of the satellite observations results in worse data quality and the VOC inventories are scarce.

Despite all the years that CH_2O has been a scientific target, very few studies have been performed in remote areas (Platt et al., 1979; Lowe and Schmidt, 1983; de Serves 1994; Arlander et al., 1995, Riedel et al., 1999; Mahajan et al., 2010; Vigouroux et al., 2018) since determining its presence and vertical distribution in the remote troposphere is indeed an instrumental challenge. Several studies have addressed the budget of CH_2O in the free troposphere from airborne observations (Lowe et al., 1980; Arlander et a., 1995; Singh et al., 2001; Nicely et al., 2016; Anderson et al., 2017; Wolfe et al., 2019; Kluge et al., 2020) and also from measurements at high-altitude sites in The Andes (Pico Espejo, 4765 m, Schreier et al., 2016), in Mexico (Altzomoni, 3980 m; Vigouroux et al., 2018), in Reunion Island (Maïdo, 21600 m; Vigouroux et al., 2018), in the USA (Mauna Loa, 3397 m, Heikes et al. 1992; Zhou et al 1996; Cantrell et al., 1996; Vigouroux et al., 2018, and Idaho Hill, 3000 m, Fried et al., 1997; Cantrell et al., 1997; Harder et al, 1997), in The Alps (Jungfraujoch, 3580 nm, Legreid et al., 2008; Balzani Lööv et al., 2008; Franco et al., 2015, and Zugspitze, 2962 m, Leuchner et al., 2016; Schreier et al., 2016; Vigouroux et al., 2018), in the Apennines (Mt. Cimone, 2165 m, Fischer et al., 2003) and in the Canary Islands (Izaña-IZO, 2360 m, Fischer et al., 1998; de Reus et al., 2005; Salisbury et al., 2006; Vigouroux et al., 2018). Overall, these studies set the values of CH_2O in the free troposphere between 0.1 and 1 nmol mol^{-1}, with high variability depending on season (minimum in winter and maximum in summer), location and altitude, and reaching up to 5 nmol mol^{-1} in case of upslope pollution transported from the planetary boundary layer (PBL). The above-mentioned studies expanding beyond the PBL into free troposphere, report a vertical distribution of CH_2O with a decreasing profile and a weak diurnal variation in the free troposphere.

This study aims at a better understanding of the chemical composition of the free troposphere by providing observations from two different environments: from an island in the subtropical region and from the Pyrenees, more exposed to European pollution. In particular, this work reports ground-based remote sensing observations of CH_2O and BrO from two remote high-altitude sites: El Teide

(TEI, Tenerife, Canary Islands, Spain; 3570 m) and Pic du Midi (PDM, French Pyrenees; 2877 m). During two field campaigns (AMISOC-TEI and Pic du Midi-PDM) in July (TEI) and September (PDM) 2013, a MAX-DOAS instrument (Multi-Axis Differential Optical Absorption Spectroscopy; Hönninger et al., 2004; Wagner et al., 2004; Platt and Stutz, 2008) scanned the troposphere vertically in order to gain insights regarding the atmospheric composition at the measurement locations. This work first describes the field campaigns as well as the measurement sites and methodology. Then, it presents the observations to, later on, discuss the presence of CH_2O at the two mountain sites and address the upper limit of BrO at the sites during each field campaign.

2. Measurements and methods

This section describes the two field campaigns and observational sites referred to in this study, along with the measurement method during both campaigns.

2.1. Field campaigns and sites description

During July and September/October 2013, two different one-month field campaigns took place at two different remote high-altitude sites (El Teide and Pic du Midi, see Fig. 1). Given the scarcity of observations in the free troposphere (i.e., above 2000 m a.s.l.; Chevalier et al., 2007), the goal of the campaigns was to characterize the composition of that part of the atmosphere. Indeed, the possibility of performing consecutive ground-based observations from El Teide and Pic du Midi presented itself as a unique opportunity to investigate the free troposphere in two different environments (marine and continental) and in different latitudinal locations (sub-tropics and mid-latitudes). In the following, each field campaign and characteristics of the observational sites are described.

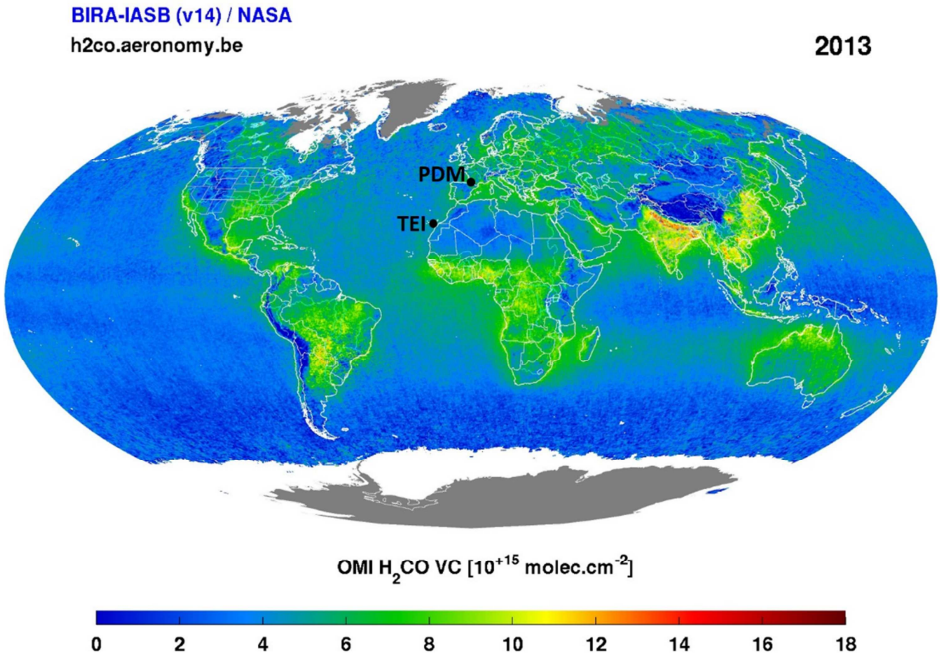

Fig. 1: Mean formaldehyde tropospheric column density during 2013 as observed from space. The observational sites referred to in this work are indicated in black (El Teide-TEI and Pic du Midi-PDM). The satellite data belong to the Ozone Monitoring Instrument (OMI) on the Aura platform (http://h2co.aeronomie.be, last access 09/11/2019).

2.1.1. AMISOC campaign at El Teide (28.27° N, 16.64° W, 3570 m a.s.l.)

Within the framework of the AMISOC research project led by INTA (Spanish National Institute for Aerospace Technology), a field campaign took place in July 2013 at the island of Tenerife (Canary Islands, Spain) in the Atlantic Ocean. The major target of the campaign was the study of the tropospheric vertical distribution of minor species related to the ozone chemistry in an oceanic environment. The specific goal of team of the Spanish National Research Council (CSIC) within AMISOC was to explore the presence and vertical distribution of UV-absorbing trace gases such as halogen oxides (BrO) and VOCs (CH_2O) in the remote free troposphere in the sub-tropics.

In collaboration with INTA and the Izaña Atmospheric Research Center (IARC) from the State Meteorological Agency of Spain (AEMET, Cuevas et al., 2017), the CSIC team installed a MAX-

DOAS instrument at El Teide (TEI) from 7th July until 1st August 2013. The instrument was mounted on a hut nearby the upper cable car station of El Teide National Park, approximately 1200 m above the Izaña Observatory (IZO, IARC), and ~150 m below the summit of the volcano El Teide.

TEI sits at a very dry environment under high insolation most of the year. Although TEI itself is not a permanent measurement site, multiple atmospheric observations have been performed for decades at IZO (i.e., ~1 km below TEI). These investigations describe IZO as free troposphere background conditions. The site is usually above the temperature inversion layer, and periodically impacted by the Saharan Air Layer, mainly in summer (Cuevas et al., 2013, 2017; Rodríguez et al., 2011; García et al., 2014). Indeed, IZO is a well-established and characterized research center that is part of the World Meteorological Organization-Global Atmospheric Watch Programme (WMO-GAW) and its predecessor Background Atmospheric Pollution Monitoring Network (BAPMoN) since 1984. IZO also contributes to several international research networks such, e.g., the AErosol RObotic NETwork (AERONET), the Network for the Detection of Atmospheric Composition Change (NDACC) or the Total Carbon Column Observing Network (TCCON) (Cuevas et al., 2015).

2.1.2. Pic du Midi campaign (42.93° N, 0.13° E, 2877 m a.s.l)

From 15th September until 13th October 2013, the same MAX-DOAS instrument from AMISOC was deployed at the Pic du Midi Observatory (PDM) in the French Pyrenees. The goal of the campaign, organized by the University of Toulouse, was to investigate the oxidation pathways of mercury (Hg) in the free troposphere. As in AMISOC, the specific goal of the CSIC-DOAS observations was to assess the presence of reactive compounds such as halogens (BrO) or aldehydes (CH_2O) in the free troposphere, this time in the mid-latitudes. During the campaign, the MAX-DOAS measurements were performed from the facilities of the Atmospheric Research Laboratory at PDM, along with observations of Hg, CO and O_3 (Marusczak et al., 2017).

The PDM (http://p2oa.aero.obs-mip.fr/) is part of the *Observatoire Midi-Pyrénées* and is a GAW station since 2018, offering long-term astronomical and atmospheric observations since the 19th century. From an air quality point of view, the site is defined as “mostly remote” (Henne et al. 2010) and, since PDM sits on top of the Pic du Midi de Bigorre and hence 1300 m above the surrounding area, the location has often been used as a remote location for free-tropospheric observations (Marenco et al. 1994). Under predominant westerly winds, the PDM generally receives humid air masses from the Atlantic Ocean. Warming of the surrounding plains leads to up-slope winds during daytime, carrying pollutants (Hg, CO, black carbon) up to the PDM (Fu et al., 2016). During nighttime, the PDM katabatic winds bring free tropospheric air to the PDM,

providing a window into the middle and upper free troposphere (2-8 km, Marenco et al. 1994; Gheusi et al., 2011; Fu et al. 2016).

2.2. Remote sensing method

The MAX-DOAS instrument deployed during both campaigns consisted of two units (indoor and outdoor units) and it was previously described in the work of Prados-Roman et al. (2015) and references therein. Thus, only a brief description is provided here. In summary, through a scanning telescope and a 10 m long optic fiber bundle, the scattered skylight of the sunlit atmosphere was directed from the weatherproof outdoor unit to the indoor unit. The latter consisted of a Princeton CCD camera and a 0.5 m Czerny-Turner spectrometer with mobile mirrors and a 600 groove/nm grating on a rotating turret. That turret was automatically moved every 25 min in order to change the diffracting angle so we could gather spectra in the UV and in the Vis range. In this work, only UV data will be referred to. The set-up yielded an instrumental field of view (FOV) of 0.5° and a spectral resolution of 0.5 nm (FWHM). Figure 2 shows the outdoor units as deployed at each site.

Although the concept of the measurement routine scanning the atmosphere at discrete elevation angles from the limb to the zenith was the same during both campaigns, the details were slightly different depending on the location. In the case of the deployment at TEI, the instrument FOV azimuth angle was fixed at 62º (0° is North) and the chosen scanning elevation angles above the instrument plane were -1, 0, 1, 2, 3, 5, 10, 30, 70 and 90 degrees (~3minutes/scan). In the case of PDM set-up, the azimuth angle of the MAX-DOAS instrument was 195º while the elevation angles were set to -2, -1, 0, 1, 2, 20 and 90º (~2 minutes/scan). Note that in both cases, the MAX-DOAS observations were performed only for solar zenith angles (SZA) lower than 70º (SZA 90° is overhead sun), minimizing possible contribution of stratospheric trace gases to the retrieval of the aimed tropospheric constituents.

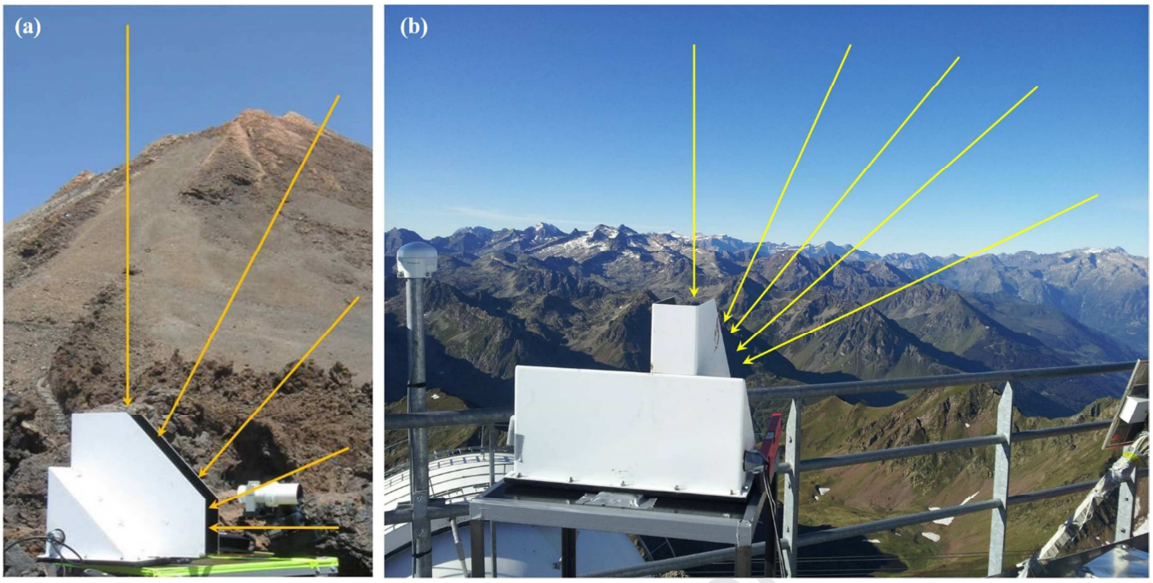

Fig. 2: Outdoor unit of the MAX-DOAS instrument installed at the two research sites. At Tenerife (a), the outdoor unit of the instrument was mounted on the roof of a hut at 3570 m a.s.l., just below El Teide's summit (3718 m a.s.l., shown in the photograph). At the Pyrenees (b), the instrument was placed on the roof of the Atmospheric Chemistry Platform at the PDM (2877 m a.s.l.), with the field of view towards the South (195°). In both cases, through a rotating mirror inside the outdoor unit, the atmosphere was scanned vertically from the limb to the zenith.

2.2.1. Spectral retrieval of trace gases

The procedure for the DOAS (Differential Optical Absorption Spectroscopy; Platt and Stuzt, 2008) spectral retrieval of the trace gases was the same for both datasets and the software used for the spectral retrieval in both campaigns was QDOAS (Danckaert et al., 2017). Following the settings suggested by Pinardi et al. (2013) where the authors performed a thorough comparison and validation exercise for MAX-DOAS observations, the spectral retrieval of CH_2O was performed in the 336.5-359 nm spectral window (further details are provided in Table 1). An example of the spectral fit is shown in Fig. 3.

In the case of TEI observations, due to saturation issues, the spectra acquired at elevation angles of 90° and at SZA < 20º were filtered out and not used at all (i.e., no observations between noon and 2:30 pm). As for the analysis procedure, the spectra were analyzed against the spectra with the higher elevation angle of each scan (i.e., 70° in TEI, 90° in PDM). In the case of the PDM campaign in the Pyrenees, where weather conditions were highly variable, the PDM-DOAS data were cloud-filtered. This was not needed in the cloud-free conditions of the TEI campaign. Further details on the data quality filtering are provided in the Supplementary Material.

Table 1: Summary of the settings used for the spectral retrieval of CH_2O (after Pinardi et al., 2013).

Parameter	Specification
Absorption cross sections	
CH_2O	Meller and Moortgat (2000)
O_3	Bogumil et al. (2003)
NO_2	Vandaele et al. (1996)
BrO	Fleischmann et al. (2004)
O_4	Thalman and Volkamer (2013)
Ring	QDOAS (Chance and Spurr, 1997)
Closure term	5^{th} order polynomial
Wavelength calibration	Based on reference solar spectrum (Chance and Kurucz, 2010)
Intensity offset	Linear

In addition to CH_2O, the presence of BrO in the free troposphere was also investigated at both high-altitude sites. Using the same absorption cross sections as those for the CH_2O spectral retrieval (Table 1), the BrO DOAS analysis was performed in three different spectral windows: in the classical two BrO absorption bands (346 - 359 nm) suggested by Aliwell at el. (2002), in the 336.5-359 nm range covering 4 bands (i.e., window of the CH_2O retrieval) and, based on the work of Franco et al. (2015), also in the region of 328.5-359 nm (i.e., 6 BrO absorption bands) where the correlation between the BrO and CH_2O absorption cross sections is minimum. Moreover, the BrO retrieval in those windows was also tested by fixing CH_2O to the average slant column density inferred at each station. Despite several tests, there was no positive spectral detection of BrO (i.e., no signatures above the residual of the DOAS fit). Hence in this work only upper limits of BrO at each site are reported (Sect. 3.1). Note that excluding the BrO cross section of the CH_2O spectral fit decreased the CH_2O differential slant column densities (dSCD) in only 1 % (within the 15 % mean error of the CH_2O dSCD, see Supplementary Material). Similarly, including the water absorption (Polyansky et al., 2018) in the spectral fit of CH_2O does not affect the retrieved CH_2O dSCD (refer to the Supplementary Material).

In order to invert the retrieved dSCD at the different elevation angles into the vertical distribution of the target gases, additional information regarding the light path is needed. The standard method for MAX-DOAS observations is to retrieve the O_2-O_2 collision induced absorption (i.e., O_4; Thalman and Volkamer et al., 2013) since its vertical distribution is known in the atmosphere. In this work, the spectral retrieval of O_4 was performed between 339-367 nm using the same absorption cross sections as for CH_2O (Table 1).

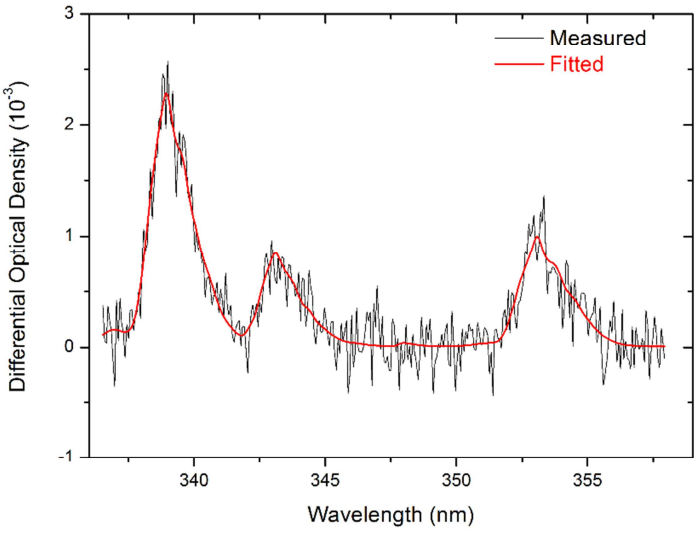

Fig. 3: Example of the DOAS spectral fit of CH_2O. The measurement was taken on 19th July 2013 at TEI (10:30 UTC) for an elevation angle of 0º. The fit of the absorption cross sections is provided in red while the measured features are shown in black. The retrieved CH_2O dSCD correspond to $3.76 \cdot 10^{16}$ molec cm^{-2} (RMS = $1.88 \cdot 10^{-4}$).

2.2.2. Inversion of vertical profile distribution

The inversion of the vertical profile distribution of CH_2O was performed by means of the "O_4 method" (Wagner et al., 2004; Frieß et al., 2006) in a two-step approach: (1) the vertical profile of the aerosol extinction coefficient (AEC) was first inverted from the retrieved O_4 dSCD, and (2) the obtained aerosol profile is used as input in the inversion of the trace gas vertical profile distribution. Note that only positive elevation angles ($\geq 0º$) were used in the vertical profile retrievals. These retrievals were performed with the Linearized Discrete Ordinate Radiative Transfer (LIDORT) radiative transfer model (Spurr et al, 2008) as part of the BePRO inversion algorithm (BIRA, Clémer et al. 2010), based on the Optimal Estimation Method (OEM, Rodgers, 2000). In order to use this method, measurements (S_e) and a prior (S_a) covariance matrices must be provided. S_e is a diagonal matrix whose diagonal terms correspond to the squared error coming from the DOAS fit. Diagonal elements of S_a correspond to 100% of the a priori profile when the CH_2O profiles are estimated. Diagonal values of S_a for aerosol retrieval were calculated following (Clémer et al., 2010), using a scaling factor (β) of 0.4. This method allows to capture large variations of the aerosol concentrations, as those observed at Tenerife (Cordoba-Jabonero et al., 2016) when Saharan dust intrusions take place. In both cases (CH_2O and aerosols), S_a non-diagonal elements correspond to a

Gaussian distribution (Hendrick et al., 2004) with a correlation length of 100 m. The averaging kernel matrix of the retrieval, as defined in Rodgers (2000), describes the sensitivity of the retrieved profile to the true state. Its trace provides the degrees of freedom of the retrieval. In this work, only inversions with degrees of freedom equal or higher to 1 were considered (i.e., at least a piece of information of the profiles came from the measurements and not from the a priori). The atmospheric characterization of TEI and PDM was obtained from the standard atmosphere (Anderson et al., 1986) for tropical and mid-latitudes, respectively. The considered atmospheric vertical grid consists of layers 100 m thick up to 6 km, layers 500 m thick between 6 and 8 km and equal to the standard atmosphere above. The surface albedo has been set to 0.07 for both stations. This value is typical of sea water for the UV-A spectral range (Chadysiene and Aloyzas, 2008) and it is also an intermediate value between pasture (0.0243) and limestone (0.11) for the UV radiation (Turner et al., 2018), corresponding to the observed scenarios at TEI and PDM respectively. In the radiative transfer model, aerosols were characterized through their phase moments and single scattering albedo (SSA). For TEI, these parameters were obtained from available AERONET data corresponding to the studied days. For PDM, there were no available AERONET data for the studied period, thus several reasonable values for SSA and the asymmetry parameters (γ) were tested, finally choosing those providing the best fit between simulated and calculated dSCDs (SSA=0.95, γ=0.65). Then, phase moments were calculated using Heyney-Greenstein phase functions.

For the vertical profile retrieval of aerosols extinction and CH_2O volume mixing ratio (vmr) at both stations, an a priori vertical profile exponentially decreasing with altitude was considered. This assumption is based on the fact that its photolysis (CH_2O main sink) increases with altitude as well as with the distance from the emission sources in the PBL. In addition, the concentration of OH decreases with altitude and so does the oxidation of CH_4 (CH_2O main source in the free troposphere) (Lowe et al., 1980; Arlander et al., 1995; Singh et al., 2001; Lawrence et al., 2001; Nicely et al., 2016). Aerosol optical depth (AOD) corresponding to the aerosol a priori profile was 0.01 and 0.005 for TEI and PDM, respectively. Vertical column density (VCD) values for the a priori profiles of CH_2O were $0.7 \cdot 10^{15}$ molec cm^{-2} and $1.0 \cdot 10^{15}$ molec cm^{-2} for TEI and PDM, respectively. These values of AOD and VCD provided the best fit between simulated and observed dSCDs of O_4 and CH_2O, respectively. The degrees of freedom of the vertical profiles retrieved in this work were 1.9 ± 0.2 and 1.6 ± 0.2 for CH_2O at TEI and at PDM, respectively (i.e., mean ± standard deviation); and 2.8 ± 0.4 and 2.4 ± 0.3 for the aerosol retrieval (TEI and PDM, respectively).

362 An example of a CH_2O vertical profile retrieved at TEI and at PDM, referred to also later on, is
363 shown in Fig. 4. The statistics of all the CH_2O and AEC inverted vertical profiles at each site are
364 summarized in Fig. 5.
365

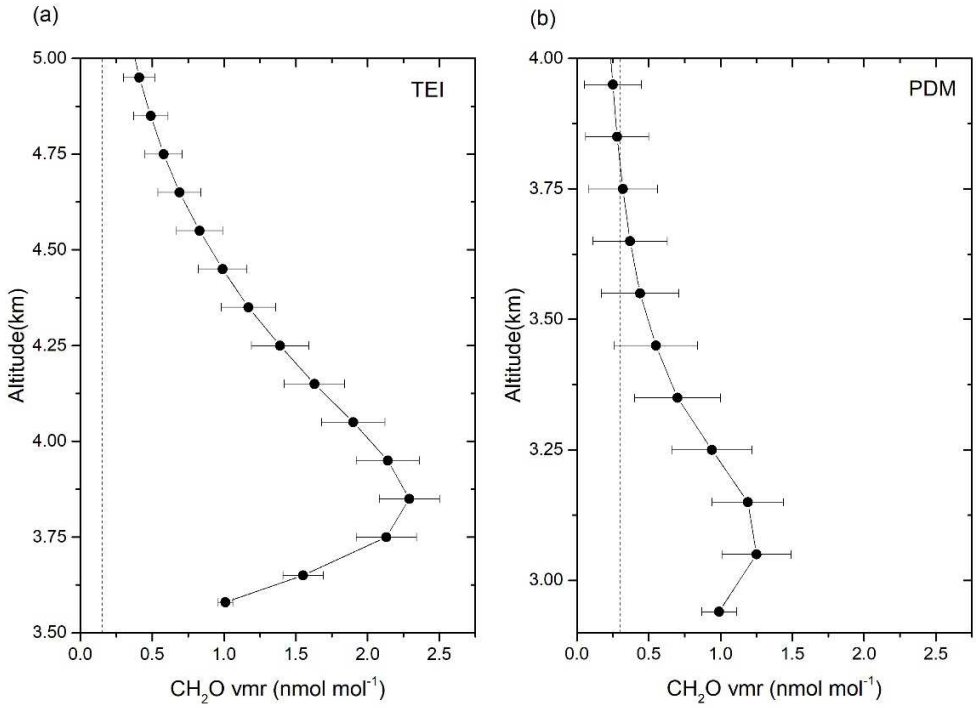

366
367 **Fig. 4**: Examples of inferred CH_2O vmr vertical profiles. The example (a) corresponds to
368 observations performed at El Teide (8th July 2013, 9 am UTC) and (b) to observations performed at
369 PDM on 26th September, 2013 (9.45 UTC). The dotted line on both plots indicates the average
370 detection limit. Note that the vertical scales are different in both plots.
371
372

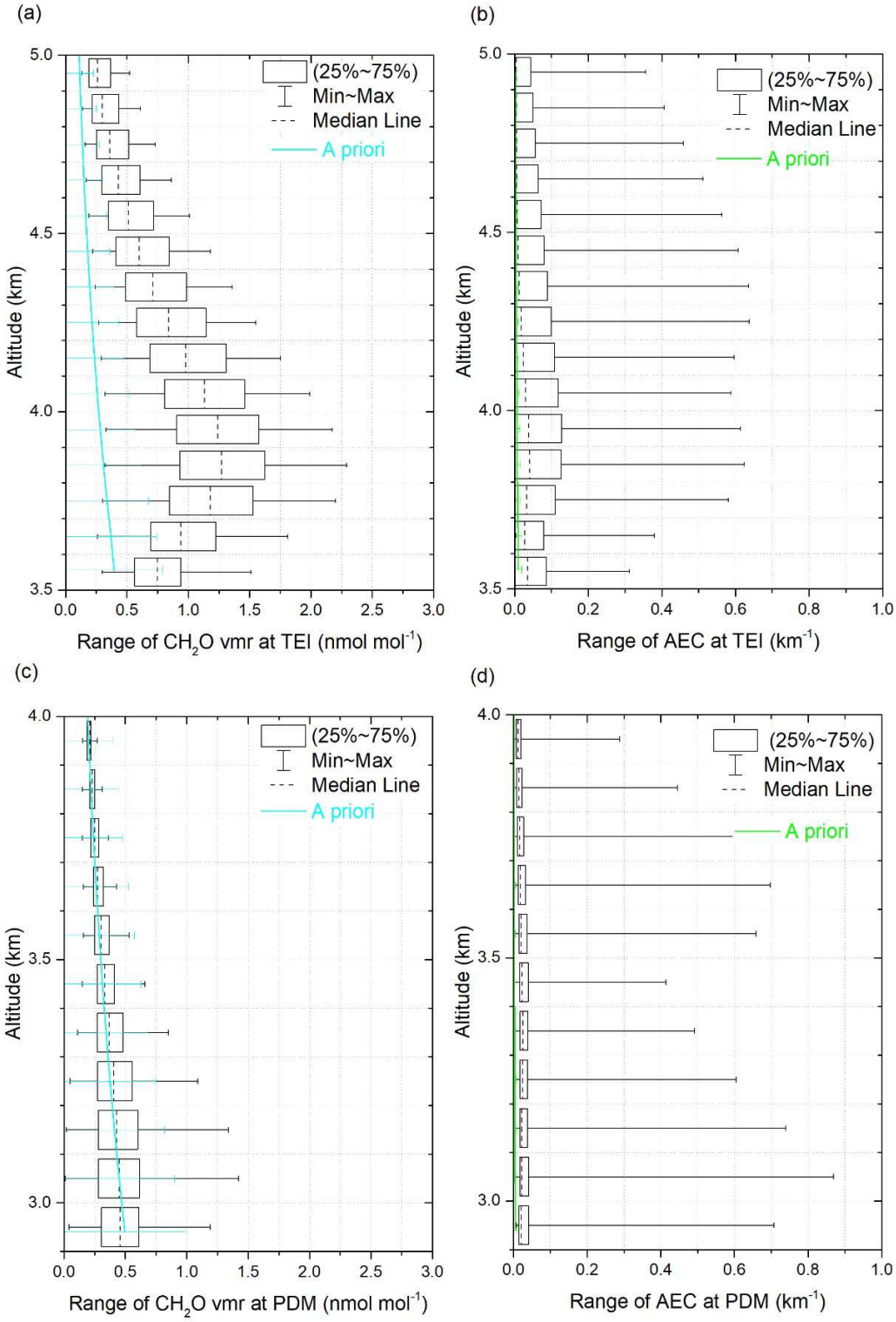

Fig. 5: Box charts of the vertical profiles of CH_2O vmr (left: a, c) and AEC (right: b, d) at TEI (up: a, b) and PDM (down: c, d) at each retrieval grid layer. Note the same vertical scales at each site. The a priori profiles for the inversion are provided in cyan (CH_2O) and green (AEC). Only cloud free data are considered.

3. Results and discussion

This section presents the vertical distribution of CH_2O and aerosol extinction coefficient retrieved at each site. Also, this section reports the BrO upper limit and discusses CH_2O observations at each site.

3.1. CH_2O and aerosol vertical distribution

The time series of the CH_2O and AEC vertical profiles during the two research campaigns are shown in Fig. 6 (TEI) and Fig. 7 (PDM). From the aerosol load point of view, both stations presented rather clear conditions although the aerosol optical depth was generally higher at TEI where a strong intrusion of Saharan dust took place on the last day of the campaign. Overall, both stations presented a mean aerosol extinction coefficient of ~0.05 km^{-1} at the instrument's altitude (0.04 km^{-1} at 3570 m at TEI, and 0.06 km^{-1} at 2877 m at PDM). At PDM, most of the extinction was located between the research site and an altitude of 4 km. However, at TEI, a higher AEC was often found above the instrument's location. As for CH_2O, the median of the retrieved mixing ratio vertical profiles indicated that, while the maximum vmr is at the instrument's altitude during the Pic du Midi campaign (0.5 ± 0.2 nmol mol^{-1} at 2.9 km a.s.l.), during AMISOC the maximum CH_2O vmr was located hundreds of meters above the instrument's altitude (0.7 ± 0.2 nmol mol^{-1} at TEI and 1.3 ± 0.3 nmol mol^{-1} at about 3.8 km a.s.l.). The mean CH_2O detection limit (i.e., double of the error of the retrieval) at the instrument's altitude was between 0.1 and 0.3 nmol mol^{-1} at both sites. Further details of the vertical profile inversion at each site and its statistics are provided in the Supplementary Materials.

As previously mentioned, unless ventilation from the PBL takes place, the vertical profile of CH_2O in the troposphere is usually assumed to decrease with altitude. While in this work this is the case for the vertical profiles retrieved at PDM, it is not the case for TEI observations. The unique distribution of CH_2O at TEI with a maintained uplifted maximum throughout AMISOC is unlikely related to upslope transport of air masses from the PBL since in summer a thick (~200 m) and strong temperature inversion (ΔT~+3ºC) associated to the top of the marine boundary layer is found between 1500 and 1800 m a.s.l. (Carrillo et al., 2016), far below TEI altitude. During AMISOC, the meteorological vertical profiles from the radiosondes launched at Güímar (Tenerife) showed these characteristics. As an example, Fig. 8 shows the Skew t –Log P diagram of the radiosonde corresponding to the 8th July 2013 (CH_2O vertical profiles of this day are shown in Fig. 4a). On this day, there was a very strong temperature inversion (ΔT~+10ºC) between ~ 860 m a.s.l. (base of the temperature inversion) and ~ 1400 m a.s.l. (top of the temperature inversion), preventing ventilation from the PBL (see Supplementary Materials with the Skew t –Log P diagram plots of the 12 UTC

411 WMO- 60018 radiosonde station corresponding to the period July 1 –August 3, 2013). Although
412 TEI itself is an arid site, a possible nearby emission of CH_2O (and/or its precursors) above the PBL
413 could be the pine forest below TEI that expands from 600 m up to 2000 m a.s.l. (Cuevas et al.,
414 2013) and could well be a source of isoprene, a biogenic VOC that produces 18% of the CH_2O
415 found globally (Bates and Jacob, 2019). However, if upslope transport of air masses takes place and
416 the origin of the CH_2O observed at TEI was solely this forest, given the high irradiation at this
417 altitude in this subtropical region, a decreasing CH_2O vertical profile would be expected with its
418 maximum located around IZO (i.e., 1.2 km bellow TEI), not 1800 m above the tree line (and over
419 300 m above TEI). Note that during similar time of the year as AMISOC, previous studies
420 performed at IZO reported on CH_2O vmr similar to the ones observed in this work at TEI's altitude
421 (i.e., no decreasing CH_2O vertical profile between IZO and TEI). With in-situ analyzers placed at
422 IZO, de Reus et al. (2005) and Salisbury et al. (2006) reported 0.65 nmol mol^{-1} mean CH_2O daily
423 values for non-dust conditions. Similar findings were made by Fischer et al. (1998), whose study
424 already pointed out the high CH_2O values observed at IZO as compared to box model results and to
425 observations at the remote site of Mauna Loa. Also, the MAX-DOAS observations do not represent
426 in-situ measurements but an average of the properties of air masses tens of kilometers away from
427 the instrument's location (Gomez et al., 2014). Thus, the CH_2O uplifted maximum detected during
428 AMISOC agrees with an advected layer around El Teide that sits at ~4 km altitude throughout July
429 2013 (i.e., just above the volcano's summit). As depicted in the 22-year study of Cuevas et al.
430 (2013), the air masses arriving at IZO during the month of July come from the west (Atlantic Ocean
431 or Canada), or from the east (from the Sahel region and the northern savannas of Africa). This is
432 also shown by the backward trajectories calculated with the HYbrid Single-Particle Lagrangian
433 Integrated Trajectory model (HYSPLIT, Stein et al., 2015, https://www.arl.noaa.gov/hysplit/, last
434 access: 09/11/2019) at TEI during AMISOC (e.g., Fig. 9, note that the backward trajectories for
435 each day are provided in the Supplementary Material). During AMISOC, during few days (7^{th}, 15^{th},
436 20^{th} and 21^{st} July) the air masses arriving at TEI's altitude crossed the Atlantic Ocean. However,
437 most of the time the air masses arriving at TEI originated from the northern savannas of Africa
438 (e.g., 8^{th} July) or from the Sahel region (e.g., 22^{th} July). In July, these two African regions are within
439 the Inter Tropical Convergence Zone (ITCZ) influence (see Supplementary Material, Fig. S3), with
440 deep convection lifting air masses straight up into the free troposphere and transporting them
441 poleward (Nicholson, 2009). Measurement and models point out these northern savannas as a
442 source region of isoprene emissions (Marais et al., 2014). As shown in Fig. 10a, during July 2013
443 the Sahel and the northern savannas of Africa suffered numerous fires, known to be strong direct
444 sources of CH_2O and its precursors. Moreover, as shown in Fig. 10b, during AMISOC absorbing

aerosols (related to biomass burning, dust and/or volcano activity, e.g., Torres et al., 1998) were detected over the North Atlantic Ocean as a result of strong Canadian fires and also carbonaceous aerosols and/or desert dust from African outflow.

The history of the vertical distribution of the air masses arriving at Tenerife during summertime is indeed quite complex. As an example, Fig. 11 (a) shows the backward trajectories of the air masses arriving at Tenerife on 31st July, 2013. While the air masses arriving at 2.5 km altitude (~IZO station) came from the free troposphere of the Sahel region, those arriving at 4 km (~TEI site) came from isoprene-rich northern savannas of Africa (with fires), and the air masses above the Teide summit came from the clean upper troposphere over the Atlantic Ocean. Note that the different air masses above and below 5 km altitude for this same day were previously reported by Dyroff et al. (2015). This sort of vertical stratification of the origin of the air masses reaching Tenerife, directed the unique behaviour of CH_2O observed during AMISOC with maximum CH_2O observed up to 500 m above the instrument's altitude (e.g., Fig, 12 b).

As for the trajectories of the air masses reaching Pic du Midi, in general they come from the Atlantic Ocean, from France or from Spain (e.g. Fig. 12, note that the backward trajectories for each day are provided in the Supplementary Material). Regardless, the air masses arrived PDM after passing over through the Pyrenees. Note that the Pyrenees and Spain are known to be strong sources of isoprene from vegetation and/or pollution (Simon et al., 2001; Simpson et al., 1995, 1999; Jiang et al., 2019). In addition, as shown in Fig. 13, the Iberian Peninsula suffered biomass burning during the measurement period at the Pyrenees. Overall, unlike at TEI, at PDM the retrieved CH_2O presented decreasing vertical profiles with a maximum value located nearby the altitude of the instrument. An example of the CH_2O retrieved at PDM is shown in Fig. 4b and the statistics of the CH_2O retrieved at PDM are provided in Fig. 5c. Further discussion on the evolution of CH_2O at both sites will be addressed in Sect. 3.2.

Regarding BrO, there was no positive detection after the DOAS retrieval and only an upper limit (i.e., double of the measurement error) of the halogen compound could be set at each high-altitude site. This was made using the RTM calculations made for Rayleigh conditions for the limb viewing direction (0º). Results indicate that the BrO upper limit at TEI during July is of 0.8 pmol mol^{-1} (at 3.5 km a.s.l.). At PDM the BrO upper limit during September was 1.5 pmol mol^{-1} (at 2.9 km a.s.l.). Note that this higher upper limit at PDM relates to worse lighting conditions compared to TEI campaign. Both BrO vmr upper limits in the free troposphere are consistent with previous studies (Volkamer et al. 2015; Wang et al. 2015).

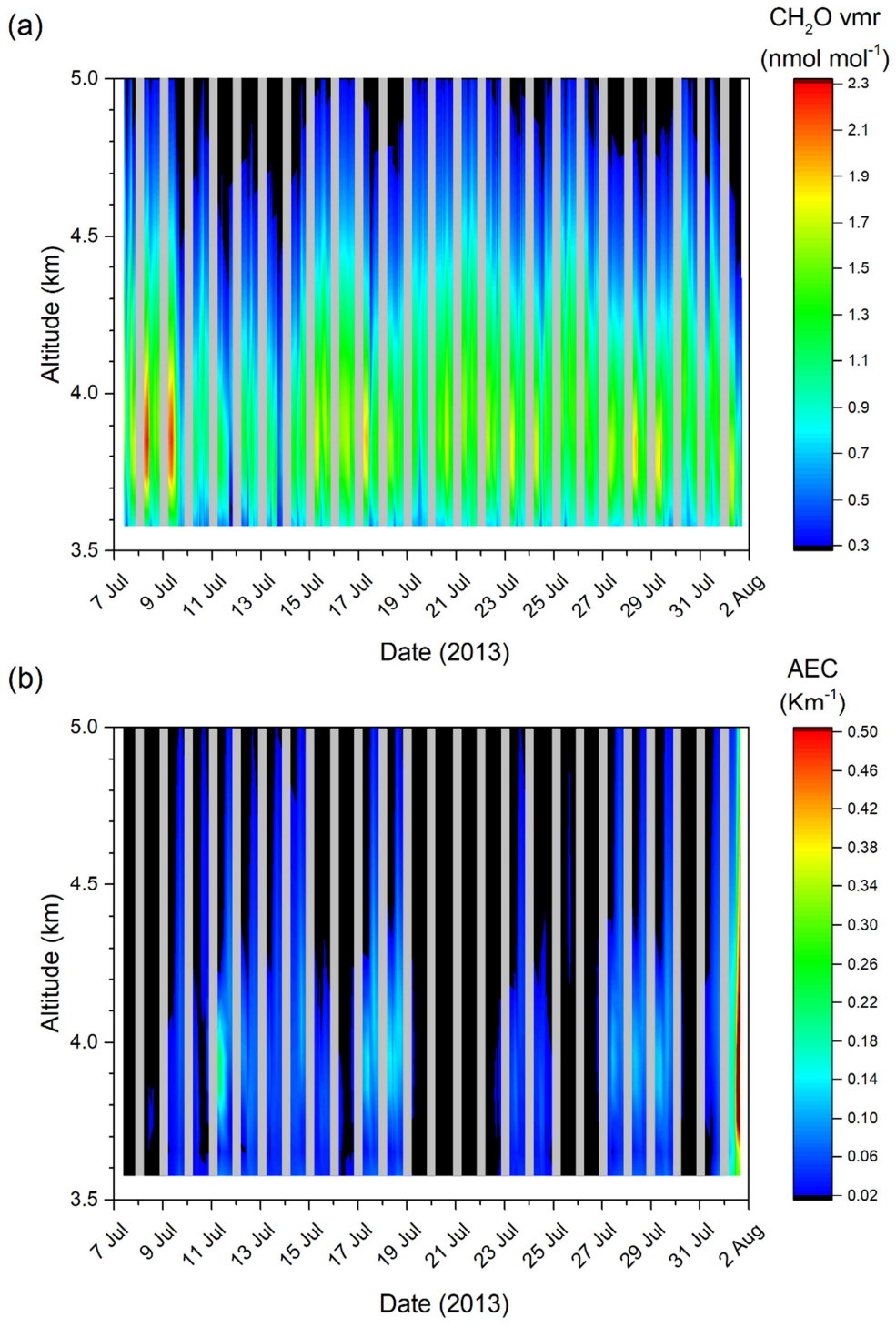

Fig. 6: CH_2O (a) and AEC (b) at El Teide. The horizontal scale shows the time period of the measurement campaign. The vertical scale indicates the altitude in the troposphere while the colour code depicts de CH_2O vmr (a) and the Aerosol Extinction Coefficient (b). The night periods when no observations were performed are shown in grey and values below detection limit in black.

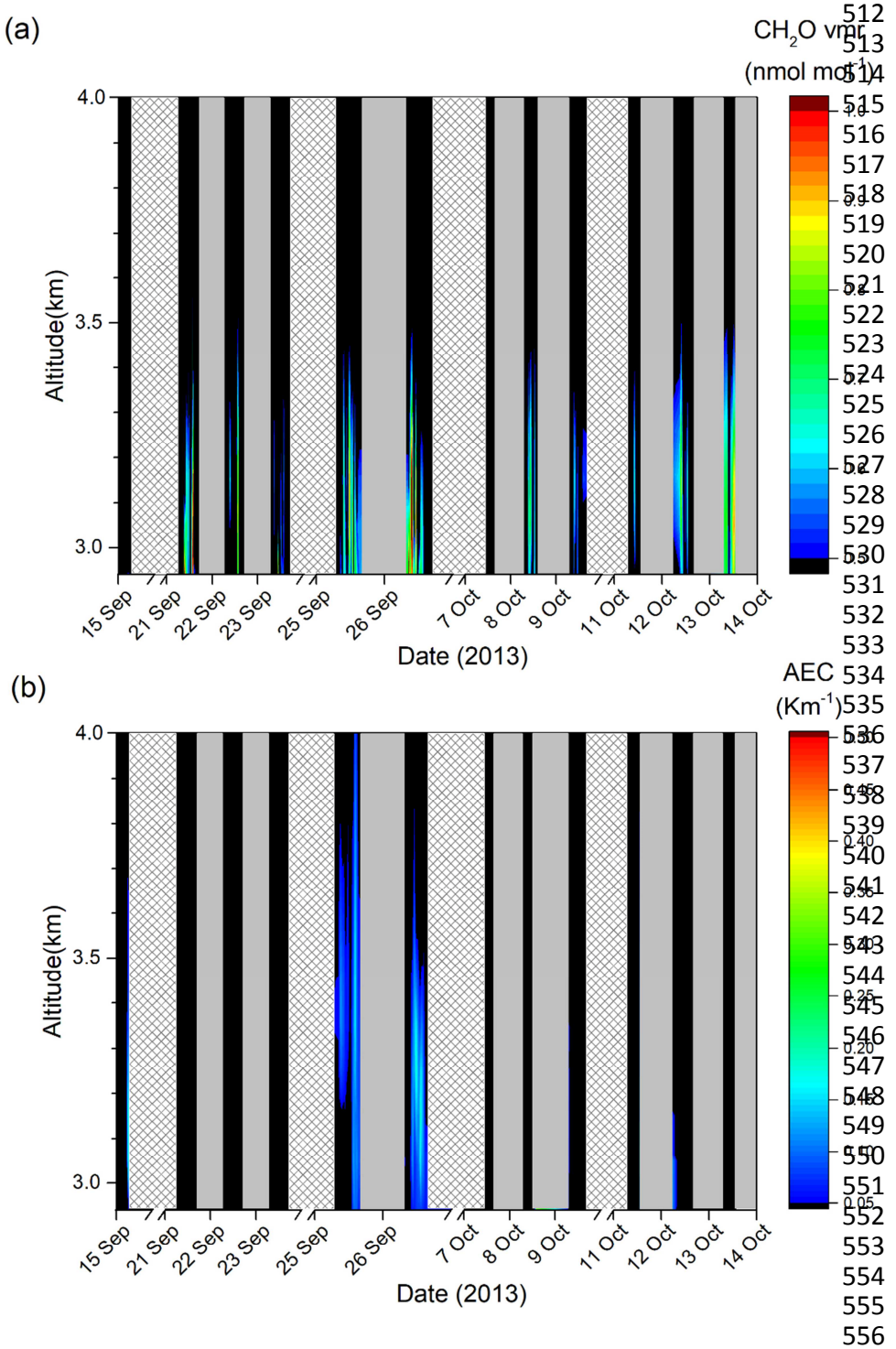

Fig. 7: CH_2O (a) and AEC (b) at Pic du Midi. The horizontal scale shows the time period of the measurement campaign. The vertical scale indicates the altitude in the troposphere while the colour code depicts de CH2O vmr (a) and the Aerosol Extinction Coefficient (b). The night periods are shown in grey, the periods with lack of measurements due to bad weather are dashed and the values below detection limit are shown in black.

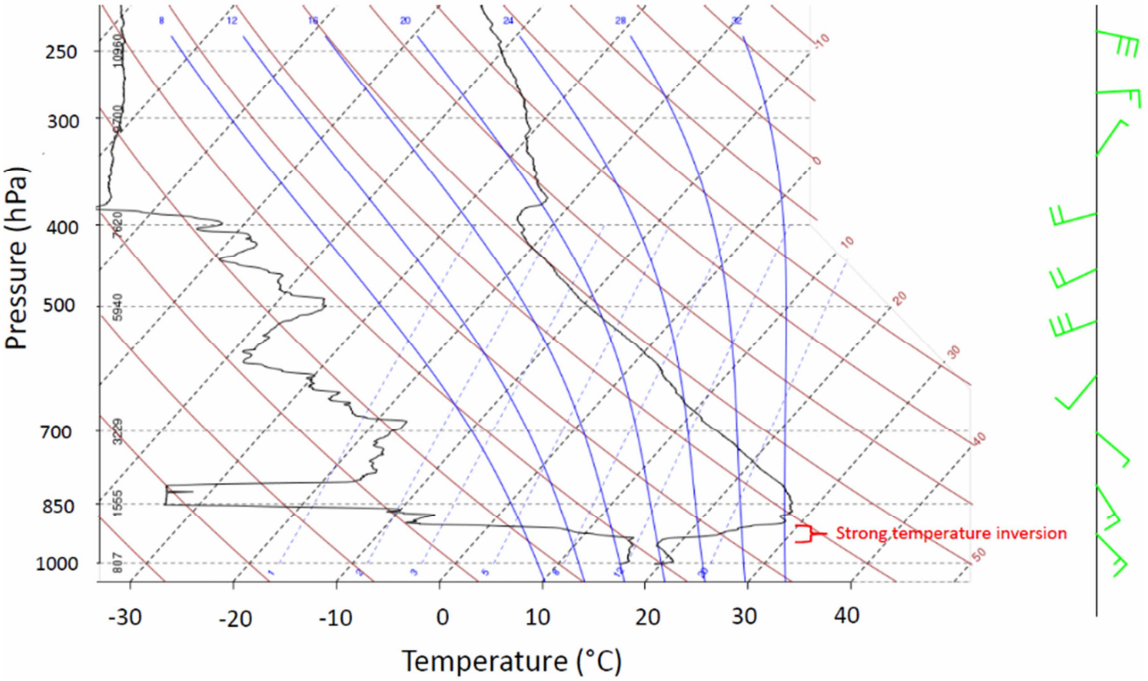

Fig. 8: Meteorological sounding corresponding to 8th July, 2013 (12 UTC, WMO- 60018 radiosonde station). Note the strong temperature inversion of $\Delta T \sim +10^{o}C$ between 1000 and 850 hPa (indicated in red). The vertical profiles of CH_2O observed this day are shown in Fig. 4a. Horizontal dashed grey lines correspond to standard pressure levels (hPa), isotherm lines (°C) are shown in right slanted dashed black, dry adiabats (°C) are given in curved brown lines, saturation adiabats (°C) are shown in blue, and saturation mixing ratios (g/kg) are shown in right slanted dashed blue lines. The left and right black lines represent the dewpoint (°C) and temperature (°C), respectively. The wind bars are provided in green.

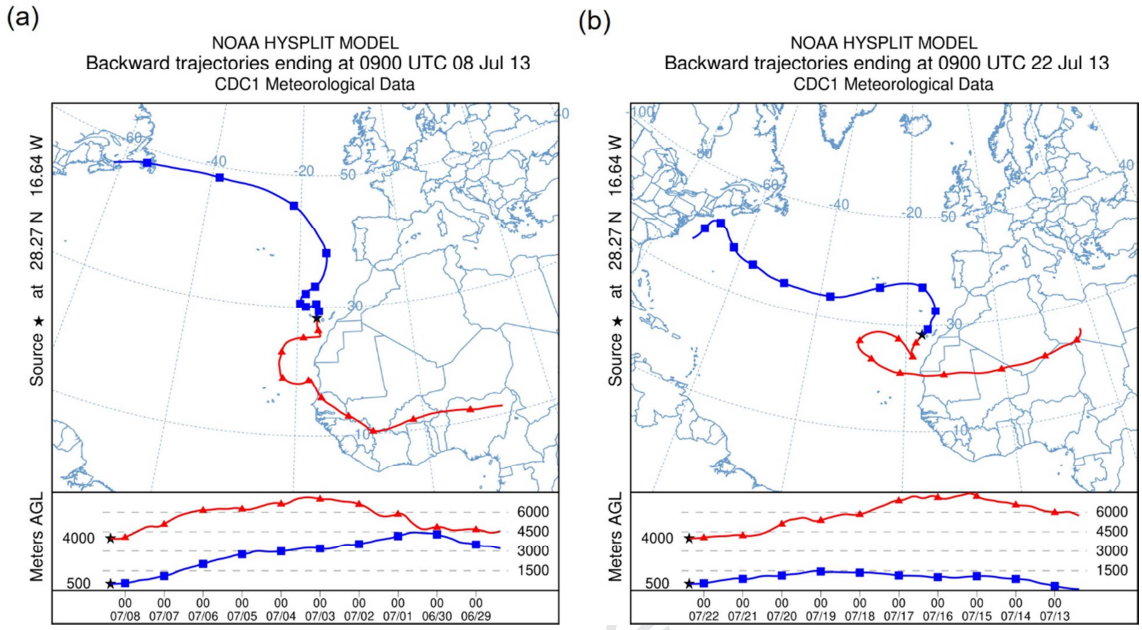

Fig. 9: 10-day backward trajectories at TEI for the 8th July (a) and for the 22th July (b), 2013. Red lines represent the backward trajectories arriving at 4 km altitude and blue lines at 500 m (a.s.l.).

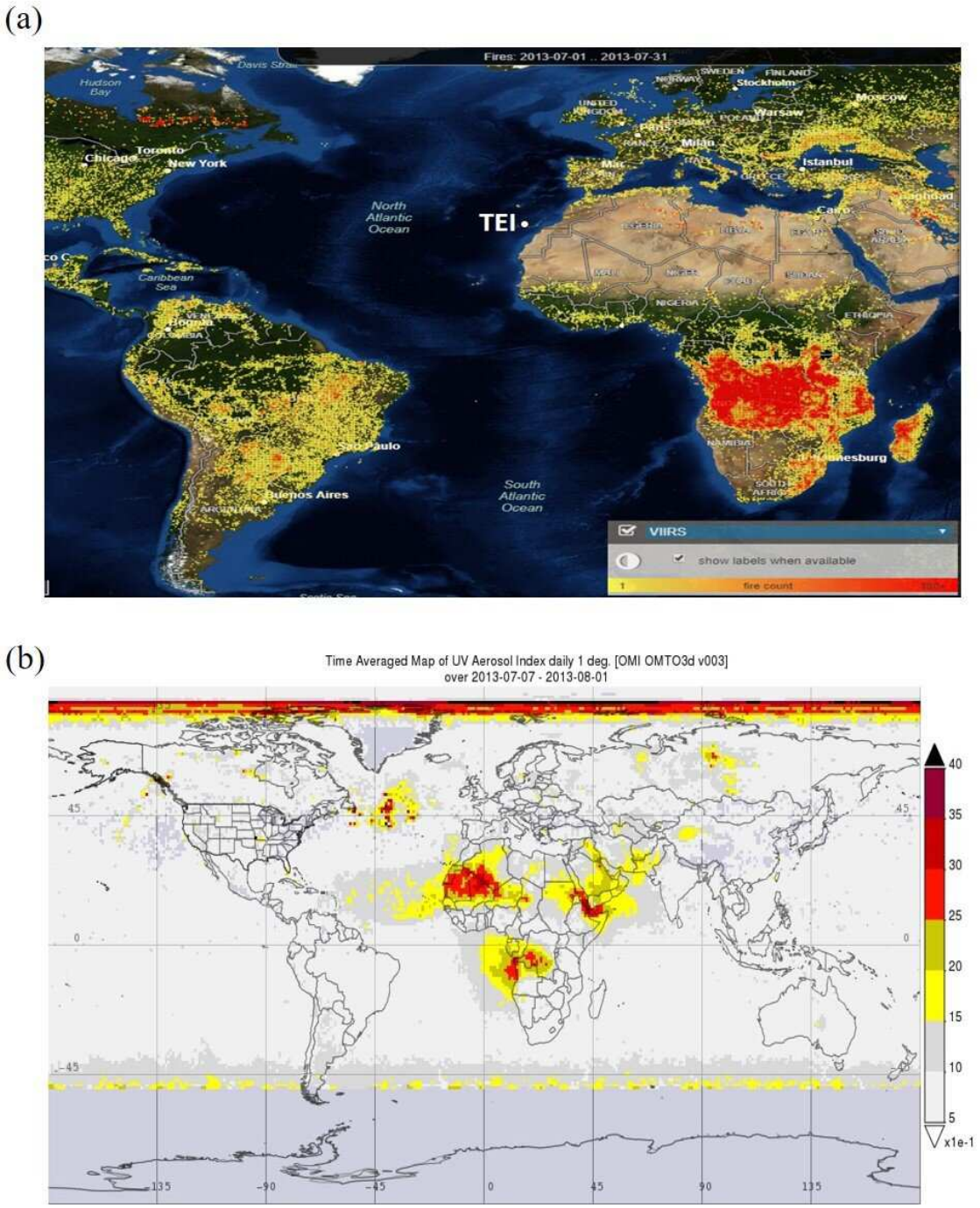

Fig. 10: Conditions during the AMISOC 2013 campaign. (a) Fire counts during July 2013. The TEI site is shown in white (Fire Information for Resource Management System, FIRMS, NASA). (b) Time averaged UV Aerosol Index (Torres et al., 1998) during AMISOC 2013 (OMTO3d, NASA Goddard Space Flight Center, Goddard Earth Sciences Data and Information Services Center, GES DISC, https://giovanni.gsfc.nasa.gov/giovanni/, last access 02/02/2020).

602

603

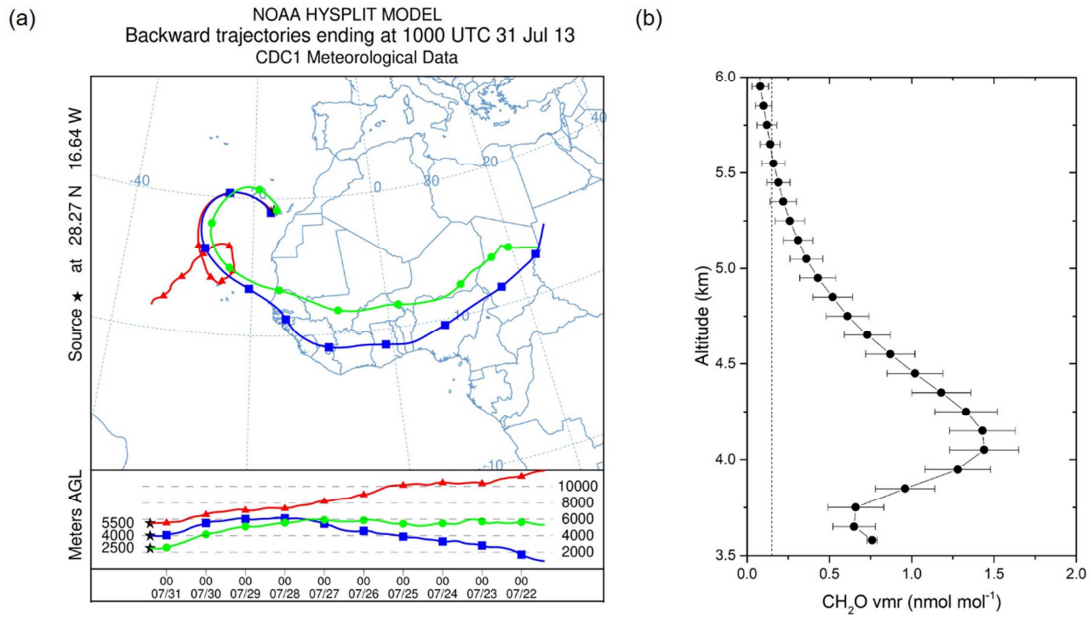

604

605 **Fig. 11**: (a) 10-day backward trajectories of the air masses arriving at 10 UTC at TEI (green), at 4
606 km (blue) and at 5.5 km (red) on 31st July, 2013. (b) Vertical distribution of the CH_2O mixing ratio
607 retrieved on that day (10.30 UTC, the dot line shows the average detection limit).

608

609

610

611

612

613

614

615

616

617

618

619

620

621

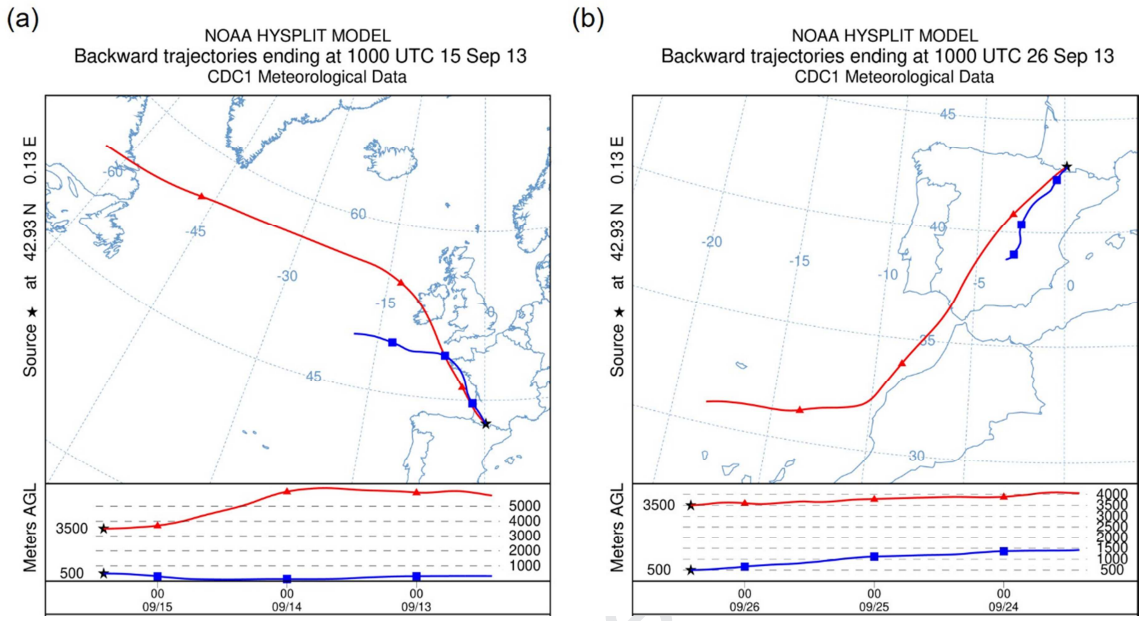

Fig. 12: 3-day backward trajectories at PDM for the 15th (a) and 26th September (b), 2013. Red lines represent the backward trajectories arriving at 3.5 km altitude and blue lines at 500 m (a.s.l.).

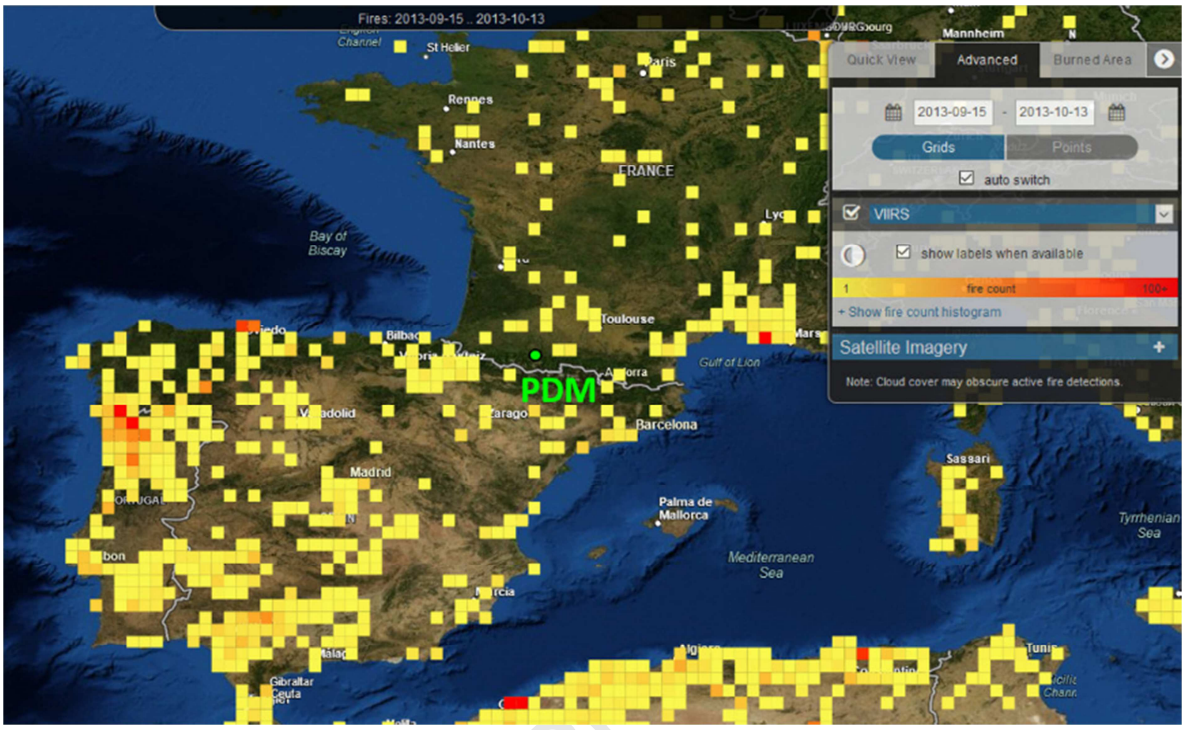

Fig. 13: Fire counts during the Pic du Midi campaign (September-October 2013). The PDM site is shown in green (Fire Information for Resource Management System, FIRMS, NASA).

3.2. Formaldehyde at each site

For a better understanding of the evolution of CH_2O in the free troposphere during each campaign, Fig. 14 shows the CH_2O mixing ratios retrieved at each site (as shown in Fig. 6 and Fig. 7), averaged over each site's location up to 1 km higher. Thus, in Fig. 14 the CH_2O vmr are averaged from TEI up to 4.5 km (mean altitude 4035 m a.s.l.) and from PDM up to 4 km (mean altitude 3438 m a.s.l). Note that these altitude ranges cover the location of the CH_2O maximum at each station and measurement time, simplifying therefore an overview of the CH_2O mixing ratio in the free troposphere at each location. Additionally, Fig. 14 also includes (in red) the amount of CH_2O expected from a simplified scheme where the main source of CH_2O in a pristine troposphere is the oxidation of background CH_4 by OH, and the main loss processes are photolysis and oxidation by OH (Equation 1-3; Platt et al., 1979):

$$CH_2O + hv \rightarrow H + HCO \ (1)$$

$$CH_2O + hv \rightarrow H_2 + CO \ (2)$$

$$CH_2O + OH \ \rightarrow H_2O + HCO \ (3)$$

For the steady state calculation given by

$$[CH_2O] = \frac{k_4[OH][CH_4]}{k_3[OH]+J_1+J_2} \ (4)$$

and shown in Fig. 14, the OH concentration, photolysis rates (J_1, J_2) and CH_4 oxidation rate (k_4) used are those reported by Zhou et al. (1996) for the high-altitude site of Mauna Loa (latitude 19.47° N) in summer (TEI) and autumn (PDM) values. The coefficient rate k_3 used is based on Platt et al. (1979) and the concentration of CH_4 used is of 1851 nmol mol^{-1}, mean value measured at IZO in 2013 with a standard deviation of less than 1% throughout the year (Cuevas et al., 2015). The concentration of OH in the troposphere is very dependent of latitude, altitude and season (e.g., Lelieveld et al., 2016; Wolfe et al., 2019). Thus, given the stability of CH_4 in a remote troposphere, OH oxidation of CH_4 and CH_2O is the main uncertainty (Δ) in this simplified estimation of steady-state CH_2O concentration. In this sense, sensitivity tests indicate that, e.g., an overestimation of 20 % in the concentration of OH used in our work (which is feasible given, for instance, the OH values reported for a mid-latitude mountain site of similar altitude as PDM, Fried et al. 1997), would lead to an overestimation of ~14 % in the amount of CH_2O in the steady-state calculation (i.e., $\Delta[CH_2O] \sim 0.7 \times \Delta[OH]$). Thus, in this case, the steady-state CH_2O values provided in Fig. 14 would represent simplified upper limits.

Regarding the CH_2O mixing ratio, Fig. 14 shows the difference between both remote sites. While the mean free tropospheric CH_2O mixing ratio in the free troposphere of the Pyrenees was 0.35 ± 0.12 nmol mol^{-1} (PDM), at the Canary Islands (TEI) it was 0.97 ± 0.26 nmol mol^{-1} (i.e., more than double). This difference could be due to the fact that the AMISOC campaign took place during summer (when CH_2O typically shows its seasonal maximum) and the Pic du Midi campaign took place in summer/autumn. However, the photolysis of CH_2O at TEI (i.e., in the subtropics and at higher altitude) is expected to be faster than at PDM. Thus, if only local sources of CH_2O are considered, the high CH_2O values observed at TEI are unexpected for a pristine high-altitude location.

As shown in Fig. 14, overall, the observed CH_2O at both sites exceeded the values expected for a pristine troposphere with background methane as main CH_2O source, which could only explain 40 % and 0.4 % of the observations at PDM and TEI, respectively. Moreover, the mean observed CH_2O values at TEI were over 3 times higher than predicted from CH_4 oxidation. But, in addition to this background CH_4, isoprene is also known to be a relevant CH_2O source producing about 20 % of the global CH_2O budget (Stavrakou et al., 2009a; Bates and Jacob, 2019). Therefore, if one considers not only background CH_4 but also that 20 % of the observed CH_2O could come from isoprene, then both background sources (i.e., methane and isoprene) could explain the observations in the Pyrenees but they could only partially explain the CH_2O values measured at TEI (51%).

The observations at the Pyrenees might be explained by NMHC transported from the PBL to PDM, like e.g. uplifted pollution from continental Spain and/or VOC emissions from the Pyrenees (Gomez and Baldasano, 1999). Indeed, Spain is a rather strong source of VOCs and particularly of isoprene from vegetation and/or pollution (Jiang et al., 2019) and, in addition to the above-mentioned fires, in September/October a thermal low is still present over the Iberian Peninsula yielding in a thick convective boundary layer (Hoinka and Castro, 2003). As for NMHC in Pic du Midi region, isoprene is emitted at a rate of 20-40 kt $month^{-1}$ during the summer/autumn season (Simpson et al., 1995). Also, Simon et al. (2001) estimated an isoprene emission of 3.6 kt y^{-1} and a total biogenic VOC emission of 3.6 kt y^{-1} from the Pyrenees. Thus, although at PDM observations and calculation agreed when considering that 20 % of the CH_2O could derive from isoprene, that contribution might be underestimated. Note that, to the authors' knowledge, this is the first time CH_2O is reported in the Pyrenees.

The observations at the Canary Islands suggest an unaccounted strong uplifted source of CH_2O. The isoprene emissions from the forest under the observation site could influence the values detected at TEI, but cannot explain the uplifted CH_2O layer encountered at Tenerife through one whole month. This uplifted layer might relate to long-range transport of CH_2O precursors (VOC emissions)

706 mainly from Africa due to synoptic scale conditions around the ITCZ (Marais et al., 2014). Indeed,
707 after a study of the trajectories followed by the different emissions from Africa during summer,
708 Meyer-Arnek et al. (2005) concluded that African air masses could be lifted up to the mid
709 troposphere and transported at high altitudes far away from their source region. They also
710 concluded that the air masses showing CH_2O enhancement further from the source region (distance
711 of days), where those affected by biomass burning (Janicot et al., 2008). Thus, NMHC emitted from
712 the biomass burning in Africa (and in Canada) and transported at high altitude to Tenerife seems a
713 reasonable source for the detected CH_2O during AMISOC. Such an uplifted layer of CH_2O and its
714 precursors transported from Africa and Canada is in agreement with the recent studies of Behrens et
715 al. (2019) and Alvarado et al. (2020). Further investigations with e.g. airborne observations would
716 be helpful to track the air masses and study the evolution and transformation of CH_2O and its
717 precursors from their source regions —such wildfires— into the free troposphere, as well as their
718 long-range transport. Indeed, the current effort of the scientific community on recent aircraft
719 campaigns encountering fire plumes such e.g. during the DC-8 ATom 2016-2018 in remote regions,
720 the HALO CAFE-2018 mission over West Africa or SouthTRAC mission in Southern America in
721 fall 2019, will tackle this issue and might also assist to improve the parametrization of chemical
722 transport models (CTMs) that could be used to assess the impact of wildfires worldwide.

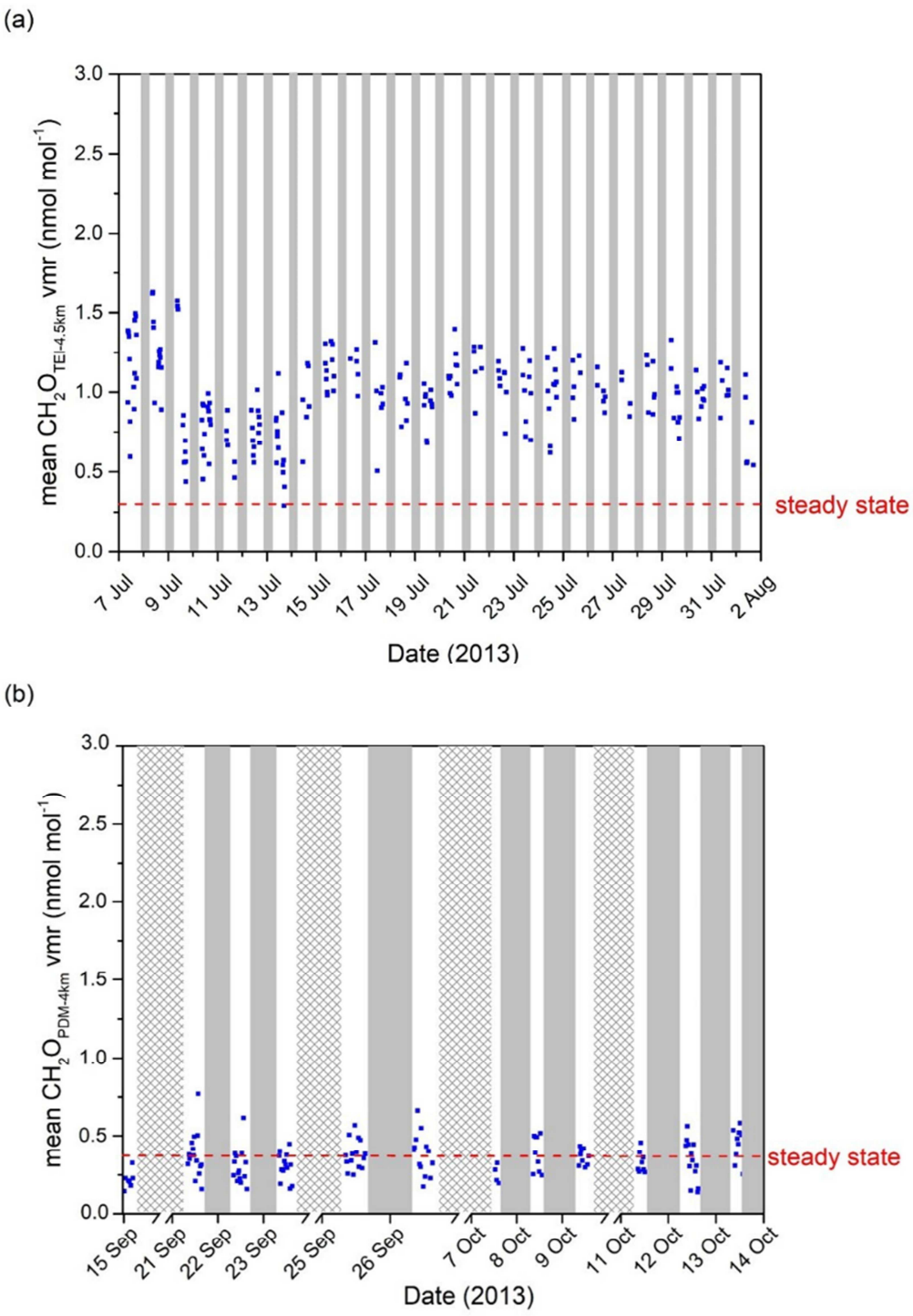

Fig. 14: Time series of the mean CH_2O mixing ratios observed at TEI (a) and PDM (b). The values are averaged within the first kilometre above each station (up to 4.5 km in TEI and up to 4 km in PDM). The night periods are given in grey, the periods with lack of measurements due to bad weather are dashed and the values below detection limit are shown in black. Formaldehyde yield from its steady state is marked in red. Note the same vertical scale at both sites.

4. Summary and conclusions

This study reports on formaldehyde (CH_2O) vertical profiles at the high-altitude sites of El Teide (Canary Islands) and Pic du Midi (French Pyrenees). Using ground-based multi-axis differential optical absorption spectroscopy during two field campaigns in July (TEI) and September (PDM) 2013, observations indicate a mean CH_2O maxima of 0.5 ± 0.2 nmol mol^{-1} at 2.9 km altitude at PDM, and an uplifted layer of CH_2O at 3.8 km at TEI (mean maxima of 1.3 ± 0.3 nmol mol^{-1}), gradually decreasing levels towards instrumental detection limit. The PDM CH_2O levels reported are slightly above levels expected from pristine environment, suggesting influence from natural and/or anthropogenic isoprene emissions (i.e., CH_2O precursor) from the Pyrenees and/or Spain. The unexpected uplifted CH_2O layer detected at TEI during the whole measurement campaign (~ 1 month), rather than the presence of a CH_2O source in the nearby region of El Teide, points towards effective recycling and long transport (convection and advection) of hydrocarbons. In agreement with recent studies, observations at TEI support the influence of wildfires (mainly African) on emission and recycling of CH_2O and its source products which, in this case, are advected and uplifted to TEI increasing the reactivity of the subtropical North Atlantic free troposphere during the summer months. The possibility of such a long-range transport of CH_2O and/or its source products should be further investigated with dedicated campaigns and CTMs. Along with investigations on CH_2O, this study also reports on reactive BrO upper limits of 0.8 and 1.5 pmol mol^{-1} at TEI and PDM, respectively. Therefore, this study contributes to broadening the knowledge of the chemical composition of the free troposphere regarding VOCs and reactive halogens in mid- and sub-tropical latitudes.

Acknowledgements

The TEI campaign was funded through the AMISOC project (Atmospheric MInor Species relevant to the Ozone Chemistry, Spanish National RCD Funding Agency, CGL2011-24891). The PDM campaign was funded by the European Research Council Executive Agency under the European Union´s Horizon 2020 Research and innovation program (ERC-2010-STG 258537) to JES. LGM would like to the MINECO support under grant VHODCA (CTM2017-83199P). The authors would like to thank the assistance of the personal working at the Izaña and at the Pic du Midi observatories. The authors acknowledge the NOAA Air Resources Laboratory (ARL) for the provision of the HYSPLIT transport and READY website (http://www.ready.noaa.gov) used in this publication. Also, we acknowledge the use of the aerosol product (AOD) from AERONET (http://aeronet.gsfc.nasa.gov/.) and the fire counts imagery from LANCE FIRMS operated by

NASA's Earth Science Data and Information System (ESDIS) with funding provided by NASA Headquarters. The UV aerosol index visualization used in this work was produced with the Giovanni online data system, developed and maintained by the NASA GES DISC. We also acknowledge the OMI mission scientists and associated NASA personnel for the production of the UV aerosol index data used in this study (Bhartia P. K. 2012, OMTO3d-OMI/Aura TOMS-Like Ozone, Aerosol Index, Cloud Radiance Fraction L3 1 day 1 degree x 1 degree V3)

References

Aliwell, S., Van Roozendael, M., Johnston, P., Richter, A., Wagner, T., Arlander, D., Burrows, J., Fish, D., Jones, R., Tørnkvist, K., Lambert, J.-C., Pfeilsticker, K., and Pundt, I.: Analysis for BrO in zenith-sky spectra: An intercomparison exercise for analysis improvement, J. Geophys. Res., 107, 1–20, doi:10.1029/2001JD000329, 2002.

Alvarado, L. M. A., Richter, A., Vrekoussis, M., Hilboll, A., Kalisz Hedegaard, A. B., Schneising, O., and Burrows, J. P.: Unexpected long-range transport of glyoxal and formaldehyde observed from the Copernicus Sentinel-5 Precursor satellite during the 2018 Canadian wildfires, Atmos. Chem. Phys., 20, 2057–2072, https://doi.org/10.5194/acp-20-2057-2020, 2020.

Anderson, D. C., Nicely, J. M., Wolfe, G. M., Hanisco, T. F., Salawitch, R. J., Canty, T. P., Dickerson, R. R., Apel, E. C., Baidar, S., Bannan,T. J., et al.: Formaldehyde in the Tropical Western Pacific: Chemical Sources and Sinks, Convective Transport, and Representation in CAM-Chem and the CCMI Models, Journal of Geophysical Research: Atmospheres, 122, 11201-11226, https://doi.org/10.1002/2016JD026121, 2017.

Anderson, G. P., Clough, S. A., Kneizys, F. X., Chetwynd, J. H., and Shettle, E. P.: AFGL atmospheric constituent profiles (0–120 km), Tech. rep., AFGL-TR-86-0110, Environmental Research papers No. 954, 1986.

Andreae, M. O. and Merlet, P.: Emission of trace gases and aerosols from biomass burning, Global Biogeochem. Cy., 15, p55–966, 2001.

Arlander, D. W., Brüning, D., Schmidt, U., and Ehhalt, D. H.: The tropospheric distribution of formaldehyde during TROPOZ II, J. Atmos. Chem., 22, 251–268, 1995.

Balzani Lööv, J. M., Henne, S., Legreid, G., Staehelin, J., Reimann,S., Prévôt, A. S. H., Steinbacher, M., and Vollmer, M. K.: Esti-mation of background concentrations of trace gases at the SwissAlpine site Jungfraujoch (3580 m asl), J. Geophys. Res.-Atmos.,113, D22305, https://doi.org/10.1029/2007JD009751, 2008.

824 Bates, K. H. and Jacob, D. J.: A new model mechanism for atmospheric oxidation of isoprene:
825 global effects on oxidants, nitrogen oxides, organic products, and secondary organic aerosol,
826 Atmos. Chem. Phys., 19, 9613–9640, https://doi.org/10.5194/acp-19-9613-2019, 2019.
827 Bauwens, M., Stavrakou, T., Müller, J.-F., De Smedt, I., Van Roozendael, M., van der Werf, G. R.,
828 Wiedinmyer, C., Kaiser, J. W., Sindelarova, K., and Guenther, A.: Nine years of global
829 hydrocarbon emissions based on source inversion of OMI formaldehyde observations, Atmos.
830 Chem. Phys., 16, 10133-10158, doi:10.5194/acp-16-10133-2016, 2016.
831 Behrens, L. K., Hilboll, A., Richter, A., Peters, E., Alvarado, L. M. A., Kalisz Hedegaard, A. B.,
832 Wittrock, F., Burrows, J. P., and Vrekoussis, M.: Detection of outflow of formaldehyde and glyoxal
833 from the African continent to the Atlantic Ocean with a MAX-DOAS instrument, Atmos. Chem.
834 Phys., 19, 10257–10278, https://doi.org/10.5194/acp-19-10257-2019, 2019.
835 Bogumil, K., Orphal, J., Homann, T., Voigt, S., Spietz, P., Fleischmann, O. C., Vogel, A.,
836 Hartmann, M., Bovensmann, H., Frerik, J., and Burrows, J. P.: Measurements of molecular
837 absorption spectra with the SCIAMACHY Pre-Flight Model: Instrument characterization and
838 reference spectra for atmospheric remote sensing in the 230–2380 nm region, J. Photochem.
839 Photobiol. A, 157, 167–184, ISSN 1010-6030, http://dx.doi.org/10.1016/S1010-6030(03)00062-5,
840 2003.
841 Cantrell, C. A., Shetter, R. E., Gilpin, T. M., and Calvert, J. G.:Peroxy radicals measured during
842 Mauna Loa Observatory Photo-chemistry Experiment 2: The data and first analysis, J.
843 Geophys.Res., 101, 14643–14652, https://doi.org/10.1029/95JD01698,1996.
844 Cantrell, C. A., Shetter, R. E., Calvert, J. G., Eisele, F. L.,Williams, E., Baumann, K., Brune, W. H.,
845 Stevens, P. S., andMather, J. H.: Peroxy radicals from photostationary state de-viations and steady
846 state calculations during the TroposphericOH Photochemistry Experiment at Idaho Hill, Colorado,
847 1993,J. Geophys. Res., 102, 6369, doi:10.1029/96JD01703, 1997.
848 Carrillo, J., Guerra, J. C., Cuevas, E., and Barrancos, J.: Characteri-zation of the Marine Boundary
849 Layer and the Trade-Wind Inver-sion over the Sub-tropical North Atlantic, Bound.-Lay. Meteo-rol.,
850 158, 311–330, https://doi.org/10.1007/s10546-015-0081-1,2016.
851 Chadysiene, R. and Alyozas, G.: Ultraviolet radiation albedo of natural surfaces, Journal of
852 Environmental Engineering and Landscape Management, 16(2), 83-88, doi: 10.3846/1648-
853 6897.2008.16.83-88, 2008.
854 Chance, K. V. and Spurr, R. J. D.: Ring effect studies: Rayleigh scattering, including molecular
855 parameters for rotational Raman scattering, and the Fraunhofer spectrum, Appl. Optics, 36, 5224–
856 5230, 1997.

857 Chance, K., P. Palmer, R. J. D. Spurr, R. V. Martin, T. P. Kurosu, and D. J. Jacob: Satellite
858 observations of formaldehyde over North America from GOME, Geophys. Res. Lett., 27, 3461–
859 3464, doi: 10.1029/2000GL011857, 2000.
860 Chance, K. and Kurucz, R.: An improved high-resolution solar reference spectrum for earth's
861 atmosphere measurements in the ultraviolet, visible, and near infrared, J. Quant. Spectrosc. Ra.,
862 111, 1289–1295, https://doi.org/10.1016/j.jqsrt.2010.01.036, 2010.
863 Chevalier, A., Gheusi, F., Delmas, R., Ordóñez, C., Sarrat, C., Zbinden, R., Thouret, V., Athier, G.,
864 and Cousin, J.-M.: Influence of altitude on ozone levels and variability in the lower troposphere: a
865 ground-based study for western Europe over the period 2001–2004, Atmos. Chem. Phys., 7, 4311-
866 4326, doi:10.5194/acp-7-4311-2007, 2007.
867 Clémer, K., Van Roozendael, M., Fayt, C., Hendrick, F., Hermans, C., Pinardi, G., Spurr, R.,Wang,
868 P., and De Mazière, M.: Multiple wavelength retrieval of tropospheric aerosol optical properties
869 from MAXDOAS measurements in Beijing, Atmos. Meas. Tech., 3, 863–878,
870 https://doi.org/10.5194/amt-3-863-2010, 2010.
871 Córdoba-Jabonero, C., Andrey-Andrés, J., Gómez, L., Adame, J.A., Sorribas, M., Navarro-Comas,
872 M., Puentedura, O., Cuevas, E., and Gil-Ojeda, M.: Vertical mass impact and features of Saharan
873 dust intrusions derived from ground-based remote sensing in synergy with airborne in-situ
874 measurements, Atmos. Environ., 142, 420–429, https://doi.org/10.1016/j.atmosenv.2016.08.003,
875 2016.
876 Crutzen, P. J.: Tropospheric ozone: An overview, in: Tropospheric Ozone, edited by: I.S.A. Isaksen,
877 D. Reidel Publ. Co., 3–32, 1988.
878 Cuevas, E., González, Y., Rodríguez, S., Guerra, J. C., Gómez-Peláez, A. J., Alonso-Pérez, S.,
879 Bustos, J., and Milford, C.: Assessment of atmospheric processes driving ozone variations in the
880 subtropical North Atlantic free troposphere, Atmos. Chem. Phys., 13, 1973-1998,
881 https://doi.org/10.5194/acp-13-1973-2013, 2013.
882 Cuevas, E., Milford, C., Bustos, J. J., del Campo Hernández, R., García, O. E., García, R. D.,
883 Gómez-Peláez, A. J., Ramos, R., Redondas, A., Reyes, E., Rodríguez, S., Romero-Campos, P. M.,
884 Schneider, M., Belmonte, J., Gil-Ojeda, M., Almansa, F., Alonso-Pérez, S., Barreto, A., González-
885 Morales, Y., Guirado-Fuentes, C., López-Solano, C., Afonso, S., Bayo, C., Berjón, A., Bethencourt,
886 J., Camino, C., Carreño, V., Castro, N. J., Cruz, A. M., Damas, M., De Ory-Ajamil, F., García, M.
887 I., Fernández-de Mesa, C. M., González, Y., Hernández, C., Hernández, Y., Hernández, M.bA.,
888 Hernández-Cruz, B., Jover, M., Kühl, S. O., López-Fernández, R., López-Solano, J., Peris, A.,
889 Rodríguez-Franco, J. J., Sálamo, C., Sepúlveda, E. and Sierra, M.: Izaña Atmospheric Research
890 Center Activity Report 2012-2014. (Eds. Cuevas, E., Milford, C. and Tarasova, O.), State

Meteorological Agency (AEMET), Madrid, Spain and World Meteorological Organization, Geneva, Switzerland, NIPO: 281-15-004-2, WMO/GAW Report No. 219, 2015.

Cuevas, E., A.J. Gómez-Peláez, S. Rodríguez, E. Terradellas, S. Basart, R.D. García, O.E. García, S. Alonso-Pérez: The pulsating nature of large-scale Saharan dust transport as a result of interplays between mid-latitude Rossby waves and the North African Dipole Intensity, Atmospheric Environment, 167, 586-602, ISSN 1352-2310, https://doi.org/10.1016/j.atmosenv.2017.08.059, 2017.

Danckaert, T., Fayt, C., Van Roozendael , M. , De Smedt , I. , Letocart , V. , Merlaud , A. , and Pinardi , G.: QDOAS Software user manual, Belgian Institute for Space Aeronomy (BIRA-IASB), version 3.2, 2017.

de Reus, M., Fischer, H., Sander, R., Gros, V., Kormann, R., Salisbury, G., Van Dingenen, R., Williams, J., Zöllner, M., and Lelieveld, J.: Observations and model calculations of trace gas scavenging in a dense Saharan dust plume during MINATROC, Atmos. Chem. Phys., 5, 1787-1803, https://doi.org/10.5194/acp-5-1787-2005, 2005.

de Serves, C.: Gas phase formaldehyde and peroxide measurements in the Arctic atmosphere, J. Geophys. Res., 99, 25391–25398, doi:10.1029/94JD00547, 1994.

De Smedt, I., Theys, N., Yu, H., Danckaert, T., Lerot, C., Compernolle, S., Van Roozendael, M., Richter, A., Hilboll, A., Peters, E., Pedergnana, M., Loyola, D., Beirle, S., Wagner, T., Eskes, H., van Geffen, J., Boersma, K. F., and Veefkind, P.: Algorithm theoretical baseline for formaldehyde retrievals from S5P TROPOMI and from the QA4ECV project, Atmos. Meas. Tech., 11, 2395-2426, https://doi.org/10.5194/amt-11-2395-2018, 2018.

Dyroff, C., Sanati, S., Christner, E., Zahn, A., Balzer, M., Bouquet, H., McManus, J. B., González-Ramos, Y., and Schneider, M.: Airborne in situ vertical profiling of HDO / H216O in the subtropical troposphere during the MUSICA remote sensing validation campaign, Atmos. Meas. Tech., 8, 2037–2049, https://doi.org/10.5194/amt-8-2037-2015, 2015.

Fischer, H., Nikitas, C., Parchatka, U., Zenker, T., Harris, G. W., Matuska, P., Schmitt, R., Mihelcic, D., Muesgen, P., Paetz, H.- W., Schulz, M., and Volz-Thomas, A.: Trace gas measurements during the Oxidizing Capacity of the Tropospheric Atmosphere campaign 1993 at Izaña, J. Geophys. Res., 103, 13 505–13 518, 1998.

Fischer, H., Kormann, R., Klüpfel, T., Gurk, Ch., Königstedt, R., Parchatka, U., Mühle, J., Rhee, T. S., Brenninkmeijer, C. A. M., Bonasoni, P., and Stohl, A.: Ozone production and trace gas correlations during the June 2000 MINATROC intensive measurement campaign at Mt. Cimone, Atmos. Chem. Phys., 3, 725-738, https://doi.org/10.5194/acp-3-725-2003, 2003.

924 Fleischmann, O. C., Hartmann, M., Burrows, J. P., and Orphal, J.: New ultraviolet absorption cross-
925 sections of BrO at atmospheric temperatures measured by time-windowing Fourier transform
926 spectroscopy, J. Photochem. Photobiol. A, 168, 117–132, 2004.
927 Franco, B., Hendrick, F., Van Roozendael, M., Müller, J.-F., Stavrakou, T., Marais, E. A., Bovy, B.,
928 Bader, W., Fayt, C., Hermans, C., Lejeune, B., Pinardi, G., Servais, C., and Mahieu, E.: Retrievals
929 of formaldehyde from ground-based FTIR and MAX-DOAS observations at the Jungfraujoch
930 station and comparisons with GEOS-Chem and IMAGES model simulations, Atmos. Meas. Tech.,
931 8, 1733-1756, https://doi.org/10.5194/amt-8-1733-2015, 2015.
932 Fried, A., McKeen, S., Sewell, S., Harder, J., Henry, B., Goldan, P., Kuster, W., Williams, E.,
933 Baumann, K., Shetter, R., and Cantrell, C.: Photochemistry of formaldehyde during the 1993
934 Tropospheric OH Photochemistry Experiment, J. Geophys. Res., 102, 6283–6296,
935 doi:10.1029/96JD03249, 1997.
936 Frieß, U., Monks, P., Remedios, J., Rozanov, A., Sinreich, R., Wagner, T., and Platt, U.:
937 MAXDOAS O_4 measurements: a new technique to derive information on atmospheric aerosols: 2.
938 Modeling studies, J. Geophys. Res., 111, D14203, doi:10.1029/2005JD006618, 2006.
939 Fu, X., Marusczak, N., Heimbürger, L.-E., Sauvage, B., Gheusi, F., Prestbo, E. M., and Sonke, J.
940 E.: Atmospheric mercury speciation dynamics at the high-altitude Pic du Midi Observatory,
941 southern France, Atmos. Chem. Phys., 16, 5623-5639, doi:10.5194/acp-16-5623-2016, 2016.
942 García, M. I., Rodríguez, S., González, Y., and García, R. D.: Climatology of new particle
943 formation at Izaña mountain GAW observatory in the subtropical North Atlantic, Atmos. Chem.
944 Phys., 14, 3865-3881, https://doi.org/10.5194/acp-14-3865-2014, 2014.
945 GCOS, The Global Observing System for Climate: Implementation Needs, GCOS Rep. 200
946 (https://library.wmo.int/index.php?lvl=notice_display&id=19838#.XT1-8HtS_cs, last access
947 09/11/2019), World MEteorologiacal Organization (WMO), 2016.
948 Gheusi, F., Ravetta, F., Delbarre, H., Tsamalis, C., Chevalier-Rosso, A., Leroy, C., Augustin, P.,
949 Delmas, R., Ancellet, G., Athier, G., Bouchou, P., Campistron, B., Cousin, J. M., Fourmentin, M.,
950 and Meyerfeld, Y.: Pic 2005, a field campaign to investigate low-tropospheric ozone variability in
951 the Pyrenees, Atmos. Res., 101, 640–665, doi:10.1016/j.atmosres.2011.04.014, 2011.
952 Gomez, O and Baldasano, J. M.: Biogenic VOC Emission Inventory For Catalonia, Spain, WIT
953 Transactions on Ecology and the Environment vol 28, doi: 10.2495/EURO990222, 1999.
954 Gomez, L., Navarro-Comas, M., Puentedura, O., Gonzalez, Y., Cuevas, E., and Gil-Ojeda, M.:
955 Long-path averaged mixing ratios of O3 and NO2 in the free troposphere from mountain
956 MAXDOAS, Atmos. Meas. Tech., 7, 3373–3386, doi:10.5194/amt-7-3373-2014, 2014.

Harder, J. W., Fried, A., Sewell, S., and Henry, B.: Comparison of tunable diode laser and long-path ultraviolet/visible spectro-scopic measurements of ambient formaldehyde concentrations during the 1993 OH Photochemistry Experiment, J. Geophys.Res., 102, 6267–6282, doi:10.1029/96JD01731, 1997.

Heikes, B. G.: Formaldehyde and hydroperoxides at MaunaLoa Observatory, J. Geophys. Res., 97, 18001–10013,https://doi.org/10.1029/92JD00268, 1992.

Hendrick, F., Barret, B., Van Roozendael, M., Boesch, H., Butz, A., De Mazière, M., Goutail, F., Hermans, C., Lambert, J.-C., Pfeilsticker, K., and Pommereau, J.-P.: Retrieval of nitrogen dioxide stratospheric profiles from ground-based zenithsky UV-visible observations: validation of the technique through correlative comparisons, Atmos. Chem. Phys., 4, 2091–2106, https://doi.org/10.5194/acp-4-2091-2004, 2004.

Henne, S., Brunner, D., Folini, D., Solberg, S., Klausen, J., and Buchmann, B.: Assessment of parameters describing representativeness of air quality in-situ measurement sites, Atmos. Chem. Phys., 10, 3561-3581, doi:10.5194/acp-10-3561-2010, 2010.

Hoinka, K. P., and M. Castro: The Iberian thermal low, Q. J. Roy. Meteorol. Soc., 129, 1491–1511, 2003.

Hönninger, G., Friedeburg, C. V., and Platt, U.: Multi axis differential optical absorption spectroscopy (MAX-DOAS), Atmos. Chem. Phys., 4, 231–254, doi:10.5194/acp-4-231-2004, 2004.

Janicot, S., Thorncroft, C. D., Ali, A., Asencio, N., Berry, G., Bock, O., Bourles, B., Caniaux, G., Chauvin, F., Deme, A., Kergoat, L., Lafore, J.-P., Lavaysse, C., Lebel, T., Marticorena, B., Mounier, F., Nedelec, P., Redelsperger, J.-L., Ravegnani, F., Reeves, C. E., Roca, R., de Rosnay, P., Schlager, H., Sultan, B., Tomasini, M., Ulanovsky, A., and ACMAD forecasters team: Large-scale overview of the summer monsoon over West Africa during the AMMA field experiment in 2006, Ann. Geophys., 26, 2569-2595, https://doi.org/10.5194/angeo-26-2569-2008, 2008.

Jiang, J., Aksoyoglu, S., Ciarelli, G., Oikonomakis, E., El-Haddad, I., Canonaco, F., O'Dowd, C., Ovadnevaite, J., Minguillón, M. C., Baltensperger, U., and Prévôt, A. S. H.: Effects of two different biogenic emission models on modelled ozone and aerosol concentrations in Europe, Atmos. Chem. Phys., 19, 3747-3768, https://doi.org/10.5194/acp-19-3747-2019, 2019.

Kitchens, J. F., Casner, R. E., Edwards, G. S., Harward III, W. E. and Macri, B. J.: Investigation of selected potential environmental contaminants: Formaldehyde, Rep. PB-256 839, National Technical Information Service, Environmental Protection Agency, 1976 (https://cfpub.epa.gov/ols/catalog/advanced_brief_record.cfm?&FIELD1=SUBJECT&INPUT1=Trioxanes&TYPE1=EXACT&LOGIC1=AND&COLL=&SORT_TYPE=MTIC&item_count=1&item_accn=34497, last access 09/11/2019).

991 Kluge, F., Hüneke, T., Knecht, M., Lichtenstern, M., Rotermund, M., Schlager, H., Schreiner, B.
992 and Pfeilsticker, K.: Profiling of formaldehyde, glyoxal, methylglyoxal, and CO over the Amazon:
993 Normalised excess mixing ratios and related emission factors in biomass burning plumes, Atmos.
994 Chem. Phys. Discuss., https://doi.org/10.5194/acp-2020-129, in review, 2020.
995 Lathière, J., Hauglustaine, D. A., Friend, A. D., De Noblet-Ducoudré, N., Viovy, N., and Folberth,
996 G. A.: Impact of climate variability and land use changes on global biogenic volatile organic
997 compound emissions, Atmos. Chem. Phys., 6, 2129-2146, doi:10.5194/acp-6-2129-2006, 2006.
998 Lawrence, M. G., Jöckel, P., and von Kuhlmann, R.: What does the global mean OH concentration
999 tell us?, Atmos. Chem. Phys., 1, 37-49, https://doi.org/10.5194/acp-1-37-2001, 2001.
1000 Legreid, G., Folini, D., Staehelin, J., L¨o¨ov, J. B., Stein-bacher, M., and Reimann, S.:
1001 Measurements of organic trace gases including oxygenated volatile organic compounds at the high
1002 alpine site Jungfraujoch (Switzerland): Seasonal varia-tion and source allocations, J. Geophys. Res.,
1003 113, D05307, doi:10.1029/2007JD008653, 2008.
1004 Leuchner, M., Ghasemifard, H., Lüpke, M., Ries, L., Schunk, C., and Menzel, A.: Seasonal and
1005 diurnal variation of formaldehyde and its meteorological drivers at the GAW site Zugspitze.
1006 Aerosol Air Qual. Res, 16, 801-815, doi: 10.4209/aaqr.2015.05.0334, 2016.
1007 Lelieveld, J., Gromov, S., Pozzer, A., and Taraborrelli, D.: Global tropospheric hydroxyl
1008 distribution, budget and reactivity, Atmos. Chem. Phys., 16, 12477–12493,
1009 https://doi.org/10.5194/acp-16-12477-2016, 2016.
1010 Lowe, D. C., Schmidt, U., and Ehhalt, D. H.: A new technique for measuring tropospheric
1011 formaldehyde CH2O, Geophys. Res. Lett., 7, 825–828, 1980.
1012 Lowe, D. C. and Schmidt, U.: Formaldehyde (HCHO) measurements in the nonurban atmosphere,
1013 J. Geophys. Res., 88, 844–858, doi:10.1029/JC088iC15p10844,1983.
1014 Mahajan, A.S., Whalley, L.K., Kozlova, E., Oetjen, H., Mendez, L., Furneaux, K. L., Goddarad, A.,
1015 Heard, D. E., Plane, J.M.C. and Saiz-Lopez, A.: DOAS observations of formaldehyde and its
1016 impact on the HO_x balance in the tropical Atlantic marine boundary layer. J Atmos Chem 66**,** 167,
1017 https://doi.org/10.1007/s10874-011-9200-7, 2010.
1018 Marais, E. A., Jacob, D. J., Guenther, A., Chance, K., Kurosu, T. P., Murphy, J. G., Reeves, C. E.,
1019 and Pye, H. O. T.: Improved model of isoprene emissions in Africa using Ozone Monitoring
1020 Instrument (OMI) satellite observations of formaldehyde: implications for oxidants and particulate
1021 matter, Atmos. Chem. Phys., 14, 7693-7703, https://doi.org/10.5194/acp-14-7693-2014, 2014.
1022 Marenco, A., Gouget, H., Nédélec, P., and Pagès, J.-P.: Evidence of a long-term increase in
1023 tropospheric ozone from Pic du Midi data series. Consequences: Positive radiative forcing, J.
1024 Geophys. Res., 99(D8), 16 617–16 632, 1994.

1025 Marusczak, N., Sonke, J. E., Fu, X., and Jiskra, M.: Tropospheric GOM at the Pic du Midi
1026 Observatory – Correcting Bias in Denuder Based Observations, Environ. Sci. Technol., 51, 863–
1027 869, https://doi.org/10.1021/acs.est.6b04999, 2017.
1028 Meller, R. and Moortgat, G. K.: Temperature dependence of the absorption cross sections of
1029 formaldehyde between 223 and 323K in the wavelength range 225–375 nm, J. Geophys. Res., 105,
1030 7089–7101, doi:10.1029/1999JD901074, 2000.
1031 Meyer-Arnek, J., Ladstätter-Weißenmayer, A., Richter, A., Wittrock, F., and Burrows, J. P.: A
1032 study of the trace gas columns of O_3, NO_2 and HCHO over Africa in September 1997, Faraday
1033 Discuss., 130, 387–405, https://doi.org/10.1039/b502106p, 2005.
1034 Nicely, J. M., Anderson, D. C., Canty, T. P., Salawitch, R. J., Wolfe,G. M., Apel, E. C., Arnold, S.
1035 R., Atlas, E. L., Blake, N. J.,Bresch, J. F., Campos, T. L., Dickerson, R. R., Duncan, B., Em-mons,
1036 L. K., Evans, M. J., Fernandez, R. P., Flemming, J., Hall,S. R., Hanisco, T. F., Honomichl, S. B.,
1037 Hornbrook, R. S., Hui-jnen, V., Kaser, L., Kinnison, D. E., Lamarque, J. F., Mao, J.Q., Monks, S.
1038 A., Montzka, D. D., Pan, L. L., Riemer, D. D.,Saiz-Lopez, A., Steenrod, S. D., Stell, M. H., Tilmes,
1039 S., Turquety, S., Ullmann, K., and Weinheimer, A. J.: An observationally constrained evaluation of
1040 the oxidative capacity in the tropical western Pacific troposphere, J. Geophys. Res.-Atmos.,
1041 121,7461–7488, https://doi.org/10.1002/2016JD025067, 2016.
1042 Nicholson, S.E. A revised picture of the structure of the “monsoon” and land ITCZ over West
1043 Africa. Climate Dyn., 32, 1155–1171, https://doi.org/10.1007/s00382-008-0514-3, 2009.
1044 Olivier, J .G. J., Peters, J., Granier, C., P´etron, G., M¨uller, J.-F., and Wallens, S.: Present and
1045 future surface emissions of atmospheric compounds, POET Report 2, EU project EVK2-1999-
1046 00011, 2003.
1047 Palmer, P. I., Jacob, D. J., Fiore, A., Chance, K. V., Martin, R. V., Kurosu, T. P., Bey, I., Yantosca,
1048 R., Fiore, A., and Li, Q.: Mapping isoprene emissions over North America using formaldehyde
1049 column observations from space, J. Geophys. Res., 108, 4180, doi:10.1029/2002JD002153, 2003.
1050 Platt, U., Perner, D., and Pätz, H. W.: Simultaneous measurement of atmospheric CH2O, O3, and
1051 NO2 by differential optical absorption, J. Geophys. Res., 84(C10), 6329– 6335,
1052 doi:10.1029/JC084iC10p06329, 1979.
1053 Platt, U. and Stutz, J.: Differential optical absorption spectroscopy– principles and applications,
1054 Physics of earth and space environments, edited by: Guzzi, R., Lanzerotti, L. J., Imboden, D., and
1055 Platt, U., Springer Berlin Heidelberg, Berlin, Germany, 597 pp., doi:10.1007/978-3-540-75776-4,
1056 2008.
1057 Pinardi, G., Van Roozendael, M., Abuhassan, N., Adams, C., Cede, A., Clémer, K., Fayt, C., Frieß,
1058 U., Gil, M., Herman, J., Hermans, C., Hendrick, F., Irie, H., Merlaud, A., Navarro Comas, M.,

1059 Peters, E., Piters, A. J. M., Puentedura, O., Richter, A., Schönhardt, A., Shaiganfar, R., Spinei, E.,
1060 Strong, K., Takashima, H., Vrekoussis, M., Wagner, T., Wittrock, F., and Yilmaz, S.: MAX-DOAS
1061 formaldehyde slant column measurements during CINDI: intercomparison and analysis
1062 improvement, Atmos. Meas. Tech., 6, 167-185, doi:10.5194/amt-6-167-2013, 2013.
1063 Polyansky, O. L., Kyuberis, A. A., Zobov, N. F., Tennyson, J., Yurchenko, S. N., and Lodi, L.:
1064 ExoMol molecular line lists XXX: a complete high-accuracy line list for water, Mon. Not. R.
1065 Astron. Soc., 480, 2597–2608, 2018.
1066 Prados-Roman, C., Cuevas, C. A., Hay, T., Fernandez, R. P., Mahajan, A. S., Royer, S.-J., Galí, M.,
1067 Simó, R., Dachs, J., Großmann, K., Kinnison, D. E., Lamarque, J.-F., and Saiz-Lopez, A.: Iodine
1068 oxide in the global marine boundary layer, Atmos. Chem. Phys., 15, 583-593, doi:10.5194/acp-15-
1069 583-2015, 2015.
1070 Riedel, K.,Weller, R., and Schrems, O.: Variability of formaldehyde in the Antarctic troposphere,
1071 Phys. Chem. Chem. Phys., 1, 5523–5527, doi: 10.1039/A905368I, 1999.
1072 Rodgers, C.: Inverse methods for atmospheric sounding,World Scientific, Singapore, New Jersey,
1073 London, Hongkong, 2000.
1074 Rodríguez, S., Alastuey, A., Alonso-Pérez, S., Querol, X., Cuevas, E., Abreu-Afonso, J., Viana, M.,
1075 Pérez, N., Pandolfi, M., and de la Rosa, J.: Transport of desert dust mixed with North African
1076 industrial pollutants in the subtropical Saharan Air Layer, Atmos. Chem. Phys., 11, 6663-6685,
1077 https://doi.org/10.5194/acp-11-6663-2011, 2011.
1078 Salisbury, G., Williams, J., Gros, V., Bartenbach, S., Xu, X., Fischer, H., Kormann, R., de Reus,
1079 M., and Zöllner, M.: Assessing the effect of a Saharan dust storm on oxygenated organic
1080 compounds at Izaña, Tenerife (July–August 2002), J. Geophys. Res., 111, D22303,
1081 doi:10.1029/2005JD006840, 2006.
1082 Sander, S. P., Finalyson-Pitts, B. J., Friedl, R. R., Golden, D. M., Huie, R. E., Keller-Rudeck, H.,
1083 Kolb, C. E., Kurylo, M. J., Molina, M. J., Moortgat, G. K., Orkin, L. V., Ravishankara, A. R., and
1084 Wine, P. H.: Chemical Kinetics and Photochemical data for use in atmospheric studies, Evaluation
1085 number 15, NASA Panel for data evaluation, JPM Publication 06-2, Jet Propulsion Laboratory,
1086 Pasadena, 2006.
1087 Schreier, S. F., Richter, A., Wittrock, F., and Burrows, J. P.: Estimates of free-tropospheric
1088 NO2 and HCHO mixing ratios derived from high-altitude mountain MAX-DOAS observations at
1089 midlatitudes and in the tropics, Atmos. Chem. Phys., 16, 2803–2817, https://doi.org/10.5194/acp-
1090 16-2803-2016, 2016.
1091 Schroeder, J. R., Crawford, J. H., Fried, A., Walega, J., Weinheimer, A., Wisthaler, A., Müller, M.,
1092 Mikoviny, T., Chen, G., Shook, M., Blake, D. R., Diskin, G., Estes, M., Thompson, A. M., Lefer, B.

L., Long, R., Mattson, E.: Formaldehyde column density measurements as a suitable pathway to estimate near-surface ozone tendencies from space, J. Geophys. Res. Atmos., 121, doi:10.1002/2016JD025419, 2016.

Simon, V., Luchetta, L. and Torres, L.: Estimating the emission of volatile organic compounds (VOC) from the French forest ecosystem. Atmospheric Environment, 35, 115–126, 2001.

Simpson, D., Guenther, A., Hewitt, C., and Steinbrecher, R.: Biogenic emissions in Europe 1. Estimates and uncertainties, J. Geo-phys. Res., 100, 22875–22890, 1995.

Simpson, D., Winiwarter, W., Borjesson, G., Cinderby, S., Ferreiro,A., Guenther, A., Hewitt, C. N., Janson, R., Khalil, M. A. K.,Owen, S., Pierce, T. E., Puxbaum, H., Shearer, M., Skiba, U.,Steinbrecher, R., Tarrason, L., and Oquist, M. G.: Inventorying emissions from nature in Europe, J. Geophys. Res.-Atmos., 104,8113–8152, https://doi.org/10.1029/98jd02747, 1999.

Singh, H., Chen, Y., Staudt, A., Jacob, D., Blake, D., Heikes, B., and Snow, J.: Evidence from the Pacific troposphere for large global sources of oxygenated organic compounds, Nature, 410, 1078–1081, doi:10.1038/35074067, 2001.

Solberg, S., Dye, C., Walker, S. E., and Simpson, D.: Long-term measurements and model calculations of formaldehyde at rural European monitoring sites, Atmos. Environ., 35, 195–207, https://doi.org/10.1016/S1352-2310(00)00256-9, 2001.

Spurr, R.: LIDORT and VLIDORT: linearized pseudo-spherical scalar and vector discrete ordinate radiative transfer models for use in remote sensing retrieval problems, in: Light Scattering Reviews 3, Springer Praxis Books, edited by: Kokhanovsky, A., vol. 7., Springer, Berlin Heidelberg, 229–275, 2008.

Stavrakou, T., Müller, J.-F., De Smedt, I., Van Roozendael, M., van der Werf, G. R., Giglio, L., and Guenther, A.: Evaluating the performance of pyrogenic and biogenic emission inventories against one decade of space-based formaldehyde columns, Atmos. Chem. Phys., 9, 1037-1060, doi:10.5194/acp-9-1037-2009, 2009a.

Stavrakou, T., Müller, J.-F., De Smedt, I., Van Roozendael, M., van der Werf, G. R., Giglio, L., and Guenther, A.: Global emissions of non-methane hydrocarbons deduced from SCIAMACHY formaldehyde columns through 2003–2006, Atmos. Chem. Phys., 9, 3663-3679, doi:10.5194/acp-9-3663-2009, 2009b.

Stein, A. F., Draxler, R. R., Rolph, G. D., Stunder, B. J. B., Co-hen, M. D., and Ngan, F.: NOAA's HYSPLIT AtmosphericTransport and Dispersion Modeling System, B. Am. Meteorol. Soc., 96, 2059–2077, https://doi.org/10.1175/BAMS-D-14-00110.1, 2015.

Thalman, R. and Volkamer, R.: Temperature dependent absorption cross-sections of O_2-O_2 collision pairs between 340 and 630 nm and at atmospherically relevant pressure, Phys. Chem. Chem. Phys., 15, 15371–15381, doi: 10.1039/c3cp50968k, 2013.

Torres, O., Bhartia, P. K., Herman, J. R., Ahmad, Z., and Gleason, J. Derivation of aerosol properties from satellite measurements of backscattered ultraviolet radiation: Theoretical basis, *J. Geophys. Res.*, 103 (D14), 17099– 17110, doi:10.1029/98JD00900, 1998.

Turner, J. and Parisi, A. V.: Ultraviolet Radiation Albedo and Reflectance in Review: The Influence to Ultraviolet Exposure in Occupational Settings, International Journal of Environmental Research and Public Health, 15, 1507; doi:10.3390/ijerph15071507, 2018.

Vandaele, A. C., Hermans, C., Simon, P. C., Van Roozendael, M., Guilmot, J. M., Carleer, M., and Colin, R.: Fourier transform measurement of NO2 absorption cross-section in the visible range at room temperature, J. Atmos. Chem., 25, 289–305, 1996.

Vigouroux, C., Bauer Aquino, C. A., Bauwens, M., Becker, C., Blumenstock, T., De Mazière, M., García, O., Grutter, M., Guarin, C., Hannigan, J., Hase, F., Jones, N., Kivi, R., Koshelev, D., Langerock, B., Lutsch, E., Makarova, M., Metzger, J.-M., Müller, J.-F., Notholt, J., Ortega, I., Palm, M., Paton-Walsh, C., Poberovskii, A., Rettinger, M., Robinson, J., Smale, D., Stavrakou, T., Stremme, W., Strong, K., Sussmann, R., Té, Y., and Toon, G.: NDACC harmonized formaldehyde time series from 21 FTIR stations covering a wide range of column abundances, Atmos. Meas. Tech., 11, 5049–5073, https://doi.org/10.5194/amt-11-5049-2018, 2018.

Volkamer, R., Baidar, S., Campos, T. L., Coburn, S., DiGangi, J. P., Dix, B., Eloranta, E. W., Koenig, T. K., Morley, B., Ortega, I., Pierce, B. R., Reeves, M., Sinreich, R., Wang, S., Zondlo, M. A., and Romashkin, P. A.: Aircraft measurements of BrO, IO, glyoxal, NO2, H2O, O2-O2 and aerosol extinction profiles in the tropics: comparison with aircraft-/ship-based in situ and lidar measurements, Atmos. Meas. Tech., 8, 2121–2148, doi:10.5194/amt-8-2121-2015, 2015.

von Kuhlmann, R., Lawrence, M. G., Crutzen, P. J., and Rasch, P. J.: A model for studies of tropospheric ozone and non-methane hydrocarbons: Model evaluation of ozone related species, J. Geophys. Res., 108 (D23),4729, doi:10.1019/2002JD003348, 2003.

Wagner, T., Dix, B., v. Friedeburg, C., Frieß, U., Sanghavi, S., Sinreich, R., and Platt, U.: MAX-DOAS O_4 measurements: A new technique to derive information on atmospheric aerosols – Principles and information content, J. Geophys. Res.-Atmos., 109, https://doi.org/10.1029/2004JD004904, 2004.

Wang, S.-Y., Schmidt, J., Baidar, S., Coburn, S., Dix, B., Koenig,T., Apel, E., Bowdalo, D., Campos, T., Eloranta, E., Evans,M., DiGangii, J., Zondlo, M., Gao, R.-S., Haggerty, J., Hall,S., Hornbrook, R., Jacob, D., Morley, B., Pierce, B., Reeves,M., Romashkin, P., ter Schure, A., and

1159 Volkamer, R.: Active and widespread halogen chemistry in the tropical and subtropical free
1160 troposphere, P. Natl. Acad. Sci. USA, 112, 9281–9286,https://doi.org/10.1073/pnas.1505142112,
1161 2015.
1162 Wolfe, G. M., Kaiser, J., Hanisco, T. F., Keutsch, F. N., de Gouw, J. A., Gilman, J. B., Graus, M.,
1163 Hatch, C. D., Holloway, J., Horowitz, L. W., Lee, B. H., Lerner, B. M., Lopez-Hilifiker, F., Mao, J.,
1164 Marvin, M. R., Peischl, J., Pollack, I. B., Roberts, J. M., Ryerson, T. B., Thornton, J. A., Veres, P.
1165 R., and Warneke, C.: Formaldehyde production from isoprene oxidation across NOx regimes,
1166 Atmos. Chem. Phys., 16, 2597–2610, https://doi.org/10.5194/acp-16-2597-2016, 2016.
1167 Wolfe, G.M., Nicely, J. M., St. Clair, J. M., Hanisco, T. F., Liao, J., Oman, L. D., Brune, W. B.,
1168 Miller, D., Thames, A., González Abad, G., Ryerson, T. B., Thompson, C. R., Peischl, J., McKain,
1169 K., Sweeney, C., Wennberg, P. O., Kim, M., Crounse, J. D., Hall, S. R., Ullmann, K., Diskin, G.,
1170 Bui, P., Chang, C., and Dean-Day,J.: Mapping hydroxyl variability throughout the global remote
1171 troposphere via synthesis of airborne and satellite formaldehyde observations, PNAS, 116 (23)
1172 11171-11180, https://doi.org/10.1073/pnas.1821661116, 2019.
1173 Zhou, X., Lee, Y.□N., Newman, L., Chen, X., and Mopper, K.: Tropospheric formaldehyde
1174 concentration at the Mauna Loa Observatory during the Mauna Loa Observatory Photochemistry
1175 Experiment 2, J. Geophys. Res., 101(D9), 14711– 14719, doi:10.1029/95JD03226, 1996.

Highlights

- Vertical profiles of formaldehyde mixing ratios at two high-altitude remote sites
- Uplifted layer of formaldehyde above El Teide
- Long-range transport of wildfire emissions into the North Atlantic free troposphere
- Isoprene emissions from the Pyrenees and/or Spain reach Pic du Midi
- First reported observations of atmospheric formaldehyde in the Pyrenees

Declaration of interests

☒ The authors declare that they have no known competing financial interests or personal relationships that could have appeared to influence the work reported in this paper.

☐The authors declare the following financial interests/personal relationships which may be considered as potential competing interests: